ARTICLE

doi:10.1038/nature11229

Deep carbon export from a Southern Ocean iron-fertilized diatom bloom

Victor Smetacek[1,2]*, Christine Klaas[1]*, Volker H. Strass[1], Philipp Assmy[1,3], Marina Montresor[4], Boris Cisewski[1,5], Nicolas Savoye[6,7], Adrian Webb[8], Francesco d'Ovidio[9], Jesús M. Arrieta[10,11], Ulrich Bathmann[1,12], Richard Bellerby[13,14], Gry Mine Berg[15], Peter Croot[16,17], Santiago Gonzalez[10], Joachim Henjes[1,18], Gerhard J. Herndl[10,19], Linn J. Hoffmann[16], Harry Leach[20], Martin Losch[1], Matthew M. Mills[15], Craig Neill[13,21], Ilka Peeken[1,22], Rüdiger Röttgers[23], Oliver Sachs[1,24], Eberhard Sauter[1], Maike M. Schmidt[25], Jill Schwarz[1,26], Anja Terbrüggen[1] & Dieter Wolf-Gladrow[1]

Fertilization of the ocean by adding iron compounds has induced diatom-dominated phytoplankton blooms accompanied by considerable carbon dioxide drawdown in the ocean surface layer. However, because the fate of bloom biomass could not be adequately resolved in these experiments, the timescales of carbon sequestration from the atmosphere are uncertain. Here we report the results of a five-week experiment carried out in the closed core of a vertically coherent, mesoscale eddy of the Antarctic Circumpolar Current, during which we tracked sinking particles from the surface to the deep-sea floor. A large diatom bloom peaked in the fourth week after fertilization. This was followed by mass mortality of several diatom species that formed rapidly sinking, mucilaginous aggregates of entangled cells and chains. Taken together, multiple lines of evidence—although each with important uncertainties—lead us to conclude that at least half the bloom biomass sank far below a depth of 1,000 metres and that a substantial portion is likely to have reached the sea floor. Thus, iron-fertilized diatom blooms may sequester carbon for timescales of centuries in ocean bottom water and for longer in the sediments.

The Southern Ocean is regarded as a likely source and sink of atmospheric CO_2 over glacial–interglacial climate cycles, but the relative importance of physical and biological mechanisms driving CO_2 exchange are under debate[1,2]. The iron hypothesis[3], which is based on iron limitation of phytoplankton growth in extensive, nutrient-rich areas of today's oceans, is that the greater supply of iron-bearing dust to these regions during the dry glacials stimulated phytoplankton blooms that, by sinking from the surface to the deep ocean, sequestered climatically relevant amounts of carbon from exchange with the atmosphere. Twelve ocean iron fertilization (OIF) experiments carried out to test this hypothesis have provided unambiguous support for the first condition: that iron addition generates phytoplankton blooms in regions with high nutrient but low chlorophyll concentrations including the Southern Ocean[4,5]. The findings are consistent with satellite observations of natural phytoplankton blooms in these regions stimulated by dust input from continental[6] and volcanic[7] sources.

The timescales on which CO_2 taken up by phytoplankton is sequestered from the atmosphere depend on the depths at which organic matter sinking out of the surface layer is subsequently remineralized back to CO_2 by microbes and zooplankton. In the Southern Ocean, the portion of CO_2 retained within the 200-m-deep winter mixed layer would be in contact with the atmosphere within months, but carbon sinking to successively deeper layers, and finally the sediments, will be sequestered for decades to centuries or longer. Previous OIF experiments have not adequately demonstrated the fate and depth of sinking of bloom biomass[5], so it is uncertain whether mass, deep-sinking events comparable to those observed in the aftermath of natural blooms[8] also ensue from OIF blooms. Furthermore, palaeo-oceanographic proxies from the underlying sediments are ambiguous regarding productivity of the glacial Southern Ocean[1,2,9,10]. Hence, the second condition of the iron hypothesis, that OIF-generated biomass sinks to greater depths, has yet to be confirmed. The issue is currently receiving broad attention because OIF is one of the techniques listed in the geoengineering portfolio to mitigate the effects of climate change[11].

Monitoring the sinking flux from an experimental bloom requires vertical coherence between surface and deeper layers, a condition fulfilled by the closed cores of mesoscale eddies formed by meandering frontal jets of the Antarctic Circumpolar Current, which are prominent in satellite altimeter images as sea surface height anomalies[12]. An

[1]Alfred Wegener Institute for Polar and Marine Research, Am Handelshafen 12, 27570 Bremerhaven, Germany. [2]National Institute of Oceanography, Dona Paula, Goa 403 004, India. [3]Norwegian Polar Institute, Fram Centre, Hjalmar Johansens Gate 14, 9296 Tromsø, Norway. [4]Ecology and Evolution of Plankton, Stazione Zoologica Anton Dohrn, Villa Comunale, 80121-Napoli, Italy. [5]Johann Heinrich von Thünen Institute, Institute of Sea Fisheries, Palmaille 9, 22767 Hamburg, Germany. [6]Department of Analytical and Environmental Chemistry, Vrije Universiteit Brussel, Pleinlaan 2, 1050 Brussels, Belgium. [7]Univ. Bordeaux/CNRS, EPOC, UMR 5805, Station Marine d'Arcachon, 2 rue du Professeur Jolyet, F-33120 Arcachon, France. [8]Oceanography Department, University of Cape Town, Private Bag X3, Rondebosch, 7701 Cape Town, South Africa. [9]LOCEAN-IPSL, CNRS/UPMC/IRD/MNHN, 4 Place Jussieu, 75252 Paris Cedex 5, France. [10]Department of Biological Oceanography, Royal Netherlands Institute for Sea Research, PO Box 59, 1790 AB Den Burg, The Netherlands. [11]Department of Global Change Research, Instituto Mediterraneo de Estudios Avanzados, CSIC-UIB, Miquel Marques 21, 07190 Esporles, Mallorca, Spain. [12]Leibniz Institute for Baltic Sea Research Warnemünde, Seestraße 15, 18119 Rostock, Germany. [13]Bjerknes Centre for Climate Research, University of Bergen, Allegaten 55, N-5007 Bergen, Norway. [14]Norwegian Institute for Water Research, Thormøhlensgate 53 D, 5006 Bergen, Norway. [15]Department of Environmental Earth System Science, Stanford University, Stanford, California 94305, USA. [16]Helmholtz Centre for Ocean Research Kiel, Düsternbrooker Weg 20, 24105 Kiel, Germany. [17]Earth and Ocean Sciences, School of Natural Sciences, National University of Ireland, Galway, Quadrangle Building, University Road, Galway, Ireland. [18]Phytolutions GmbH, Campus Ring 1, 28759 Bremen, Germany. [19]Department of Marine Biology, University of Vienna, Althanstrasse 14, 1090 Vienna, Austria. [20]School of Environmental Sciences, University of Liverpool, Room 209 Nicholson Building, 4 Brownlow Street, Liverpool L69 3GP, UK. [21]Wealth from Oceans Flagship, Commonwealth Scientific and Industrial Research Organisation, Castray Esplanade, Hobart, Tasmania 7000, Australia. [22]MARUM – Center for Marine Environmental Sciences, University of Bremen, Leobener Strasse, D-28359 Bremen, Germany. [23]Institute for Coastal Research, Helmholtz-Zentrum Geesthacht, Center for Materials and Coastal Research, Max-Planck-Strasse 1, 21502 Geesthacht, Germany. [24]Eberhard & Partner AG, General Guisan Strasse 2, 5000 Arau, Switzerland. [25]Centre for Biomolecular Interactions Bremen, FB 2, University of Bremen, Postfach 33 04 40, 28359 Bremen, Germany. [26]School of Marine Science & Engineering, Plymouth University, Drake Circus, Plymouth PL4 8AA, UK.
*These authors contributed equally to this work.

added advantage offered by closed eddy cores is that processes occurring in the fertilized patch can be compared with natural processes in adjoining unfertilized waters of the same provenance.

The eddy and experiment

The European Iron Fertilization Experiment (EIFEX) was carried out from 11 February 2004 to 20 March 2004 during RV *Polarstern* cruise ANT XXI/3, in the clockwise-rotating core of an eddy formed by a meander of the Antarctic polar front (Fig. 1 and Supplementary Information). The eddy was mapped over a period of seven days shortly after fertilization of the patch with a grid of 80 stations along eight north–south transects 9 km apart. The rotating patch was encountered on two of the grid transects. Measurements of current speed and direction with the vessel-mounted acoustic Doppler current profiler and images of sea surface height anomalies revealed a closed, 60-km-diameter core clearly demarcated from the surrounding meander of the Antarctic polar front in all measured physical, chemical and biological properties (Fig. 1a, b and Supplementary Information).

Estimates of geostrophic shear and transports derived from temperature and salinity profiles (Supplementary Figs 1 and 2) indicate a coherent surface-to-bottom eddy circulation that was almost closed

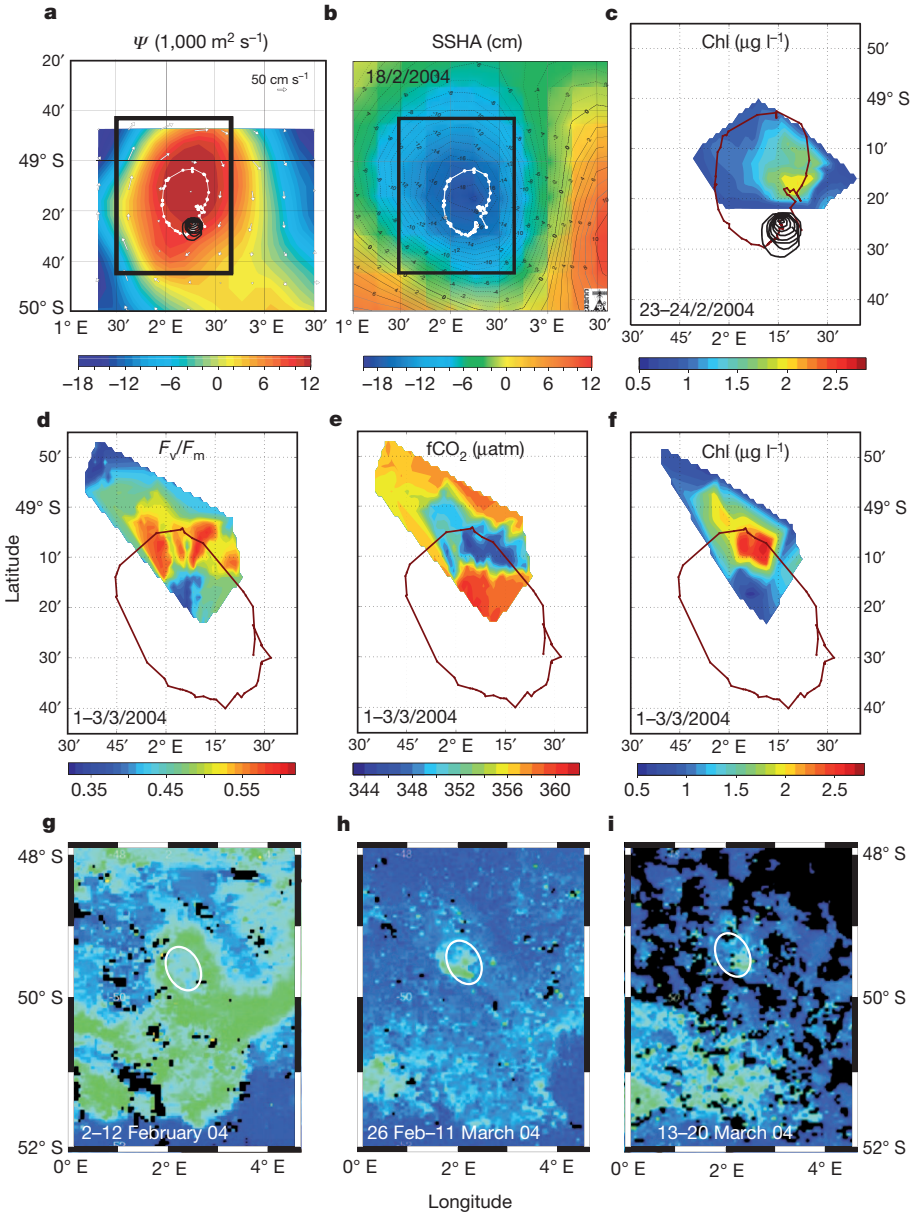

Figure 1 | Experimental eddy and the fertilized patch. **a**, The eddy core depicted with the stream function (Ψ; contours and colour scale) derived from currents measured using a vessel-mounted acoustic Doppler current profiler at a regular grid of stations between days 1 and 7. The black spiral is the ship's track (a Lagrangian circle) around the buoy drifting southwestward during fertilization. The white line is the superimposed track of the drifting buoy during its first rotation from days −1 to 11 (same as in **b** and **c**). **b**, Altimeter image of sea surface height anomaly (SSHA; contours and colour scale from CCAR, http://argo.colorado.edu/~realtime/gsfc_global-real-time_ssh/.) The rectangle in **a** and **b** is enlarged in **c**–**f**. **c**, Area and location of the patch on days 10 and 11 after fertilization, depicted on the basis of chlorophyll measurements. The yellow area is the hot spot. **d**–**f**, Location and area of the patch 17 days after fertilization, depicted in terms of photochemical efficiency (F_v/F_m; **d**), CO_2 fugacity (fCO_2; **e**) and chlorophyll concentration (**f**). The line is the track of the drifting buoy during its second rotation (days 13–21). The red area in **f** is the hot spot. **g**–**i**, Satellite-derived surface chlorophyll concentrations of the EIFEX eddy before fertilization (**g**), during the bloom peak (**h**) and in its demise phase (**i**). The eddy core is encircled in white; the EIFEX bloom is evident in **h** and **i** (green colour is >1 μg Chl l^{-1}). Note the natural bloom along the Antarctic polar front, which disappeared in this period. SeaWiFS images (**g**–**i**) courtesy of the NASA SeaWiFS Project and GeoEye.

and had little divergence. The vertical coherence of the eddy was also revealed by the congruent tracks of four neutrally buoyant floats positioned at respective depths of 200, 300, 500 and 1,000 m (Supplementary Fig. 3). A post-cruise Lagrangian analysis based on delayed-time altimetry[13] showed that, for the entire duration of the experiment, the compact core was only marginally eroded by lateral stirring, losing less than 10% of its content in total (Supplementary Information). This finding is consistent with diffusive heat budgets derived from the observed warming of the eddy's cold core[14]. Hence, the EIFEX eddy provided ideal conditions for monitoring the same water column from the surface to the sea floor over time.

The site of the pre-fertilization control station was marked with a drifting buoy around which a circular patch of 167 km^2 was fertilized with dissolved Fe(II) sulphate on 12–13 February (day 0) to yield a concentration of 1.5 μmol Fe m^{-3} in the 100-m-deep surface mixed layer, which is greater than background values by a factor of around five. A second fertilization on days 13 and 14 added an additional 0.34 μmol Fe m^{-3} to the 100-m-deep surface layer of the spreading patch. The patch was inadvertently placed off-centre but well within the closed eddy core and completed four rotations during the experiment. The area of the patch increased from 167 km^2 on day 0 to 447 km^2 on day 11 and to 798 km^2 on day 19 (Fig. 1c–f and Supplementary Information). 'In-stations' were taken in the least-diluted region of the patch: the 'hot spot' (Fig. 1c–f). 'Out-stations' were taken within the eddy core well away from the patch but in different locations relative to it, and hence did not represent ideal controls for quantifying processes within the patch.

Sampling frequency and depth coverage by discrete measurements are illustrated by the vertical distributions of chlorophyll and silicate concentrations (Fig. 2). Vertical profiles from *in situ* recording instruments indicated that the boundary of the mixed layer, defined by a sharp dip in temperature, salinity, fluorescence and transmission, was generally at a depth of 100 m (ref. 15; 97.6 ± 20.6 m). The element and biomass budgets presented here are based on inventories (in moles or grams per square metre) derived from the trapezoidal integration of six to eight discrete measurements from the 100-m-deep surface layer. For comparison with other studies, the stocks (inventories) from this layer are also presented where appropriate as depth-averaged concentrations (in millimoles or milligrams per cubic metre).

Processes inside and outside the patch

Enhanced phytoplankton growth stimulated by iron fertilization resulted in highly significant, linear increases in stocks of chlorophyll (Chl), particulate organic carbon (POC), nitrogen (PON), phosphate (POP) and biogenic silica (BSi) until day 24 (Figs 2a and 3). These stocks, depicted as depth-averaged concentrations in Fig. 3, declined thereafter, although at different rates. However, inventories of the corresponding dissolved nutrients, including dissolved organic nitrogen (DON), underwent a constant, linear decline until the end of the experiment, indicating that the respective uptake rates were maintained throughout (Fig. 3). Detailed, visual, quantitative examination of organisms and their remains across the entire size spectrum of the plankton revealed that population growth of many different species of large diatoms accounted for 97% of the Chl increase. The decline after day 24 was caused by mass death and formation of rapidly sinking aggregates by some diatom species, which was partly compensated by continued growth of other, heavily silicified species with high accumulation rates. The strikingly linear, instead of exponential, trends can be attributed to the effects of patch dilution with surrounding water because dilution rates (0.06–0.1 d^{-1}; Supplementary Information) and phytoplankton accumulation rates (0.03–0.11 d^{-1}) were similar.

The discrepancies in the budgets of particulate and dissolved pools of the various elements in the surface layer can only be explained by the sinking out of particles, as losses to dissolved organic pools can largely be ruled out: stocks of dissolved organic carbon (DOC) remained stable (44 ± 2 mmol C m^{-3}; Fig. 3l), those of DON halved (from 3.8 to 2.0 mmol N m^{-3}; Fig. 3f) and those of dissolved organic phosphate (not shown) were at the detection limit. The decline in DON was barely reflected in DOC because it was apparently associated with a relatively small, labile fraction with much lower C/N ratios than that of the large refractory DOC pool.

The post-fertilization eddy survey revealed that the patch was located in the region of the eddy core with the highest silicate and lowest chlorophyll concentrations (~0.7 mg Chl m^{-3}; Supplementary Information). Patchy, natural blooms, probably caused by local dust input along the Antarctic polar front[6], had occurred before our arrival adjacent to the patch (Fig. 1g), as indicated by lower nutrient and higher Chl stocks (up to 1.2 mg Chl m^{-3}) and higher particle loads in subsurface layers (Supplementary Information). These

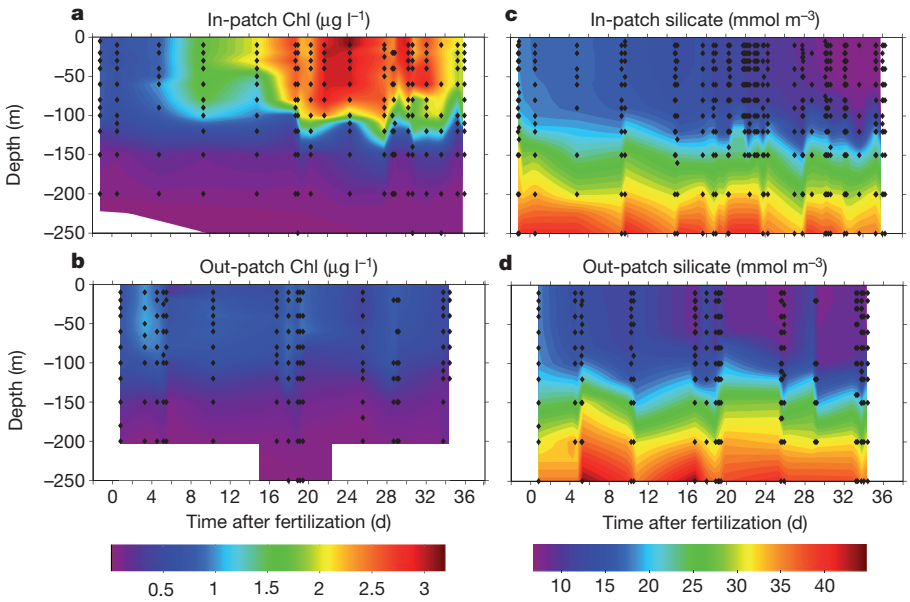

Figure 2 | Temporal evolution of chlorophyll and silicate concentrations. **a**, Chlorophyll concentrations reflect the growth, peak and demise phases of the bloom in the patch. **b**, By comparison, the Chl concentration outside the patch is low. The slightly higher out-patch values soon after fertilization are due to local patchiness in outside water and not to interim accumulation. **c**, **d**, The declining trend of silicate in outside water (**d**) is interrupted by local patchiness, whereas within the patch the trend is smooth (**c**). Note the variations in mixed-layer depth below 100 m. Black diamonds indicate depths of discrete samples.

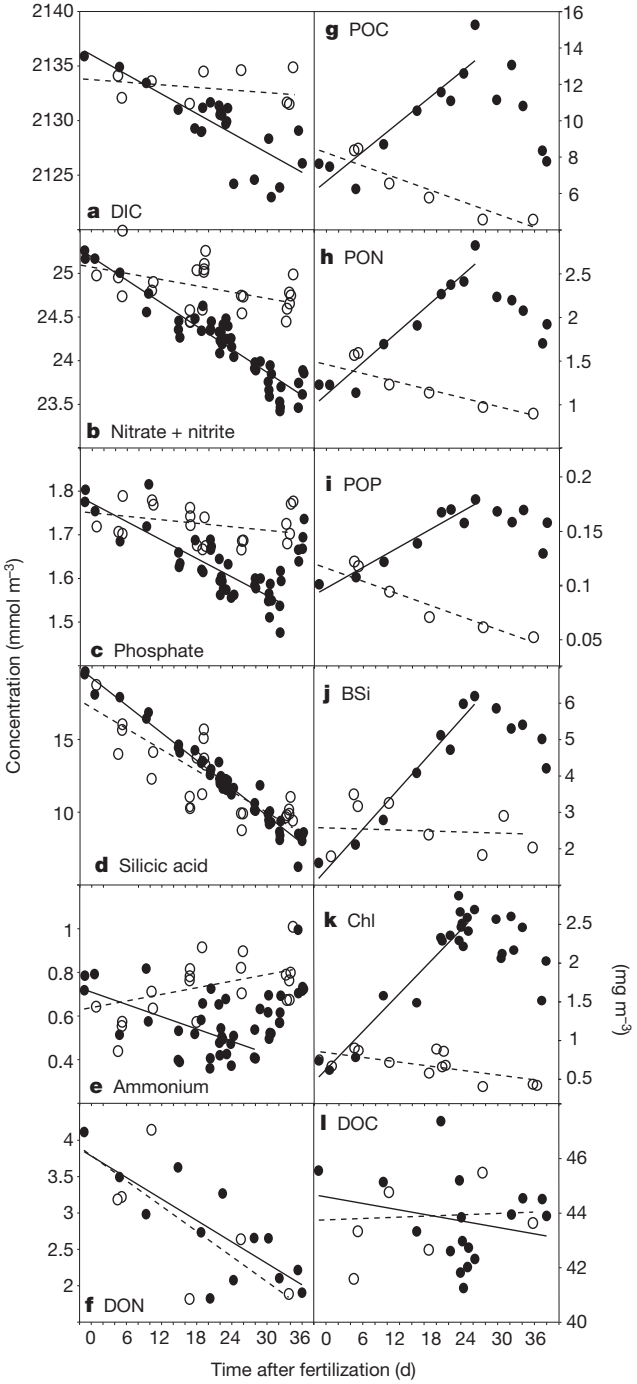

Figure 3 | Temporal evolution of dissolved and particulate elements. Values inside (filled circles) and outside (open circles) the fertilized patch are depth-integrated average concentrations for the upper 100 m of the water column. All concentrations are in millimoles per cubic metre except that for Chl (**k**), which is expressed in milligrams per cubic metre. Lines represent the temporal evolution inside (solid line) and outside (broken line) the fertilized patch used in elemental budget calculations (Supplementary Methods) determined by linear regression. Inside the patch, the r^2 values for the models are 0.64 (DIC; **a**), 0.88 (nitrate plus nitrite; **b**), 0.74 (phosphate; **c**), 0.97 (silicic acid; **d**), 0.33 (ammonium; **e**), 0.63 (DON; **f**), 0.84 (POC; **g**), 0.94 (PON; **h**), 0.93 (POP; **i**), 0.96 (BSi; **j**), 0.92 (Chl; **k**) and 0.05 (DOC; **l**). Outside the patch, the r^2 values are 0.06 (DIC), 0.24 (nitrate plus nitrite), 0.13 (phosphate), 0.71 (silicic acid), 0.24 (ammonium), 0.58 (DON), 0.84 (POC), 0.64 (PON), 0.85 (POP), 0.008 (BSi) and 0.005 (DOC). All regressions are significant ($P < 0.005$) with the exception of in-patch DOC ($P = 0.4$) and out-patch DIC ($P = 0.5$), nitrate plus nitrite ($P = 0.011$), phosphate ($P = 0.1$), ammonium ($P = 0.02$), DON ($P = 0.046$), PON ($P = 0.03$), BSi ($P = 0.8$) and DOC ($P = 0.8$).

natural blooms sank from the surface in the first week, as corroborated by barite profiles in subsurface layers[16], and, hence, greater particle stocks encountered at depth at some out-stations probably stemmed from them. Particle stocks (except those of BSi) in the upper 100-m-deep layer outside the patch continued declining by about 50% during the five weeks of the experiment (Fig. 3) as a result of steady sinking out of particles, as indicated by the discrepancy between the temporal evolutions of dissolved and particulate inventories of the respective elements. On a visit to the eddy core on day 50, we found that Chl concentrations had declined further, to 0.1 mg Chl m^{-3}.

Export from the iron-induced bloom

Vertical particle flux (export) induced by iron fertilization was estimated for the hot spot from losses of biogenic element inventories in the surface layer, including ^{234}Th; the increase in POC in the underlying deep water column; and by balancing rates of primary production and heterotrophic activity. These estimates represent the total export and include losses incurred by the surface layer in the absence of fertilization (background flux). Because some out-stations were affected by patchy natural blooms within the eddy core, they did not represent ideal controls. However, export rates from the fertilized patch, estimated from elemental budgets in the surface layer (0–100 m) and particularly POC increments between depths of 200 and 500 m until day 24, were remarkably similar to the corresponding values from outside water (Fig. 4), indicating little additional flux from the growing bloom. Export from the patch increased steeply after day 24, but outside loss rates remained constant. Hence, we assume that the background flux from the patch also remained constant until the end of the experiment but was overridden by the iron-induced flux event starting between days 24 and 28. We estimate the total background export from the patch by extrapolating the flux between days 0 and 24 to day 36, and subtract this amount from the total export to obtain the iron-induced export (Supplementary Methods).

Element losses

A conservative estimate for the export of biogenic elements from the 100-m-deep surface layer in the hot spot is the difference between the decline in dissolved inventories (nutrient uptake) and concomitant accumulation in particulate stocks (Supplementary Table 1). Uptake was calculated from the linear regressions depicted in Fig. 3a–f. Accumulation was estimated as the difference between final and initial stocks of BSi, POP, PON and POC. Initial stocks of particulate elements were taken from the intercept on day 0 of the linear regressions until day 24, and final stocks were the values measured on day 36 (Fig. 3g–j). The decline in the inventory of dissolved inorganic carbon (DIC), of 1.1 mol m^{-2}, underestimates the actual uptake by phytoplankton because of atmospheric CO_2 replenishment. Correcting for air–sea gas exchange adds 0.4 mol m^{-2} to the uptake and, hence, also to export. The background flux was obtained by extrapolating the losses estimated until day 24 (0.3 mol C m^{-2}) to the values on day 36. The iron-induced export, of 0.9 mol C m^{-2} (79 mmol C m^{-2} d^{-1} for the 12-day flux event), was obtained by subtracting the background flux from the total flux estimates (1.4 mol C m^{-2}) for the 36 days of the calculations (Supplementary Table 1).

Correcting budgets with the measured values presented above for mixed-layer deepening and diapycnal mixing using the diffusion coefficient of 3.3×10^{-4} m^2 s^{-1} estimated for the EIFEX eddy core[14] almost doubles the estimates of background export inside the hot spot (from 0.4 to 0.9 mol C m^{-2}, or 12 to 26 mmol C m^{-2} d^{-1}) and outside the fertilized patch (from 0.7 to 1.2 mol C m^{-2}, or 21 to 36 mmol C m^{-2} d^{-1}). Because nutrient input to the surface layer from below was relatively constant during the experiment, the correction for iron-induced export during the last 12 days was comparatively minor: from 0.9 to 1.1 mol C m^{-2}, or 79 to 98 mmol C m^{-2} d^{-1}. Furthermore, correcting the hot-spot budgets for the effects of

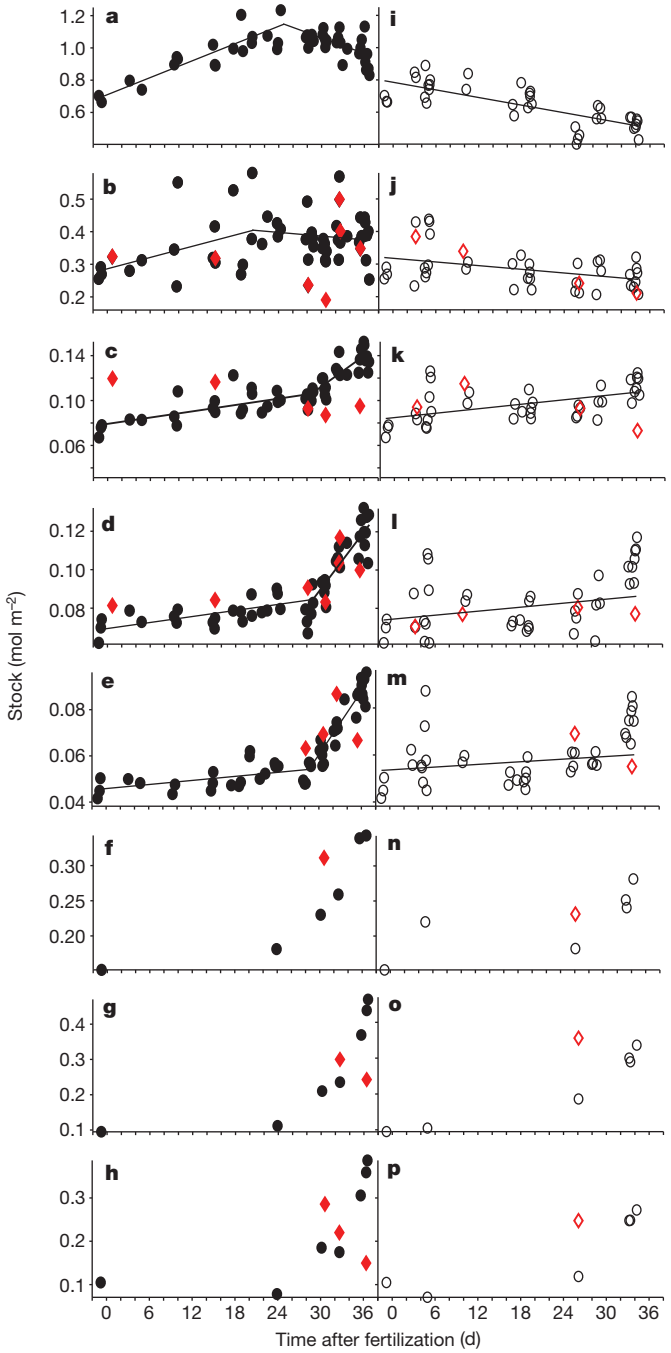

Figure 4 | Temporal evolution of particulate organic carbon stocks in successive depth layers. Stocks for the respective layers are derived from depth-integrated, vertical profiles of beam attenuation of a transmissometer calibrated using discrete POC measurements (black symbols). Filled and open symbols show data inside and outside the patch, respectively. Depth intervals of integrations are 0–100 m (**a**, **i**), 100–200 m (**b**, **j**), 200–300 m (**c**, **k**), 300–400 m (**d**, **l**), 400–500 m (**e**, **m**), 500–1,000 m (**f**, **n**), 1,000–2,000 m (**g**, **o**) and 2,000–3,000 m (**h**, **p**). Lines are derived from linear regression models. Variability in stocks and trends in the layers at 100–200 m (**b**, **j**) is due to intermittent shoaling and deepening of the particle-rich, surface mixed layer between 100 and 120 m, possibly as a result of the passage of internal waves. The high out-patch values on days 5 and 34 are not included in the regressions. The layer below 3,000 m is not included to avoid contamination by resuspended sediments in the nepheloid layer. Red diamonds show integrated stocks from measurements on discrete water samples. Variability in these values is due to low depth resolution, particularly below 500 m.

horizontal dilution (patch spreading) increases the total DIC uptake to 2.4 mol C m^{-2}, of which 0.6 mol C m^{-2} is exported laterally (Table 1). However, the increase of iron-induced export to 1.2 mol m^{-2} is again minor (Table 1). Dividing the total DIC uptake (2.4 mol C m^{-2}) by the total amount of iron added to the patch water column (0.18 mmol Fe m^{-2}) yields a C/Fe ratio of 13,000 ± 1,000 (s.e.m.). This ratio is conservative for reasons discussed in Supplementary Information.

Nitrate (nitrate plus nitrite) uptake until the bloom peak on day 24 (0.17 mol m^{-2}) accounted for 80% of PON production (0.21 mol N m^{-2}), resulting in negative values for background flux not indicated by the other elements (Supplementary Table 2). The decline in DON, through uptake by bacteria and excretion as ammonium to phytoplankton, more than compensates for the N deficit, but its origin is enigmatic. The same amount of DON, but much less DIC, nitrate and phosphate, were taken up outside the patch (Fig. 3 and Supplementary Table 3); hence DON contribution to export outside the patch is likely to have been similar to that inside the patch. The high variability in ammonium stocks (Fig. 3e) is consistent with rapid turnover within this pool. No clear trends were observed in the subsurface ammonium maxima inside and outside the patch (Supplementary Fig. 4), indicating minor additional accumulation of breakdown products from the flux event in the subsurface layer. The C/N ratio for iron-induced export (8.5) is higher than the POC/PON ratio of suspended elements (~5), a result that was also observed during the Southern Ocean Iron Experiment[4].

The steep increase in phosphate stocks on days 35 and 36 (Fig. 3c) is only partly explained by leaching from autolysed cytoplasm, owing to the well-established greater mobility of this element relative to carbon[17]. Hence, the negative value for exported P due to fertilization (Table 1) is difficult to explain, because unlike for N, the source of the additional phosphate during the last two days is unknown. Approximately 65% of the silicate taken up was exported during the 36 days, of which half can be attributed to iron-induced export at a C/Si ratio of 3 and the other half to background flux at a C/Si ratio of 0.8. Outside the patch, silicate uptake was slightly lower than inside but all of it was exported in the same period at a C/Si ratio of 0.9, which we attribute to the activity of diatom species that selectively sink silica.

POC export rates from the hot spot estimated from ^{234}Th increased steeply from background values <40 mmol C m^{-2} d^{-1} to 125 mmol C m^{-2} d^{-1} during days 28–32, but declined thereafter presumably owing to uncertainties associated with short-term sampling by this method (Supplementary Information). Nevertheless, the two peak values during the flux event are the highest recorded so far in the Southern Ocean.

Transmissometer profiles

Beam attenuation of the profiling transmissometer was highly correlated with discrete POC measurements across the entire range of concentrations encountered ($r^2 = 0.934$ and $P < 0.001$, where r is the correlation coefficient and P is the observed significance level; Supplementary Fig. 5). Because of the high-resolution vertical coverage of the water column, the depth-integrated transmissometer profiles provide a record of POC accumulation and depletion over depth and time from which export can be estimated[18].

Integrated POC stocks in the upper 3,000 m of the water column of the patch increased over 36 days by 1.3 ± 0.2 mol C m^{-2} (s.d.; Fig. 5), implying an accumulation rate of 38 mmol C m^{-2} d^{-1}. The flux event after day 24 is signalled by steeply increasing POC stocks in the water column below 200 m (Fig. 4). These stocks reached 0.8 ± 0.1 mol C m^{-2} (s.d.) above background levels on day 36, of which 0.7 ± 0.1 mol C m^{-2} (s.d.) was below 500 m (Fig. 5). The increase in deep POC stocks is reasonably close to the corrected estimate of iron-induced export from the surface layer budget (1.2 ± 0.4 mol C m^{-2} (s.d.)), given that some POC had already reached the deep-sea floor, as indicated by fresh diatom cells and labile pigments found close to the bottom (Supplementary Fig. 7). Hence, losses of iron-induced sinking flux due to ongoing respiration were apparently minor. Profiles of biogenic

Table 1 | Total and iron-induced export from the hot spot of the fertilized patch

	Days	Si	P	$NO_2 + NO_3$	Total N	C
Decrease in stocks of dissolved elements	0–36	1.14 ± 0.03	0.007 ± 0.003	0.160 ± 0.008	0.33 ± 0.08	1.1 ± 0.2
Input due to air–sea gas exchange	0–36	—	—	—	—	0.4
Dissolved-element input from vertical mixing (diapycnal mixing and deepening of the mixing layer)	0–36	0.22 ± 0.01	0.011 ± 0.0008	0.059 ± 0.004	0.10 ± 0.01	0.6 ± 0.2
Dissolved-element input from horizontal mixing (dilution effect)	0–36	~0	0.010 ± 0.001	0.061 ± 0.005	0.08 ± 0.03	0.27 ± 0.06
Total uptake (decrease in dissolved stocks plus gas exchange plus vertical mixing plus horizontal mixing)	0–36	1.36 ± 0.03	0.028 ± 0.003	0.28 ± 0.01	0.50 ± 0.09	2.4 ± 0.2
Difference between final and initial particulate-matter standing stocks	0–36	0.28 ± 0.02	0.0062 ± 0.0005	0.081 ± 0.009	0.081 ± 0.009	0.11 ± 0.07
Particulate matter loss by horizontal mixing (dilution effect)	0–36	0.19 ± 0.02	0.0089 ± 0.0004	0.110 ± 0.006	0.110 ± 0.006	0.58 ± 0.04
Vertical export (total uptake minus difference in particulate stocks minus particulate loss by horizontal mixing)	0–36	0.89 ± 0.04	0.013 ± 0.003	0.09 ± 0.02	0.31 ± 0.09	1.7 ± 0.2
Background (vertical) export*	0–36	0.50 ± 0.07	0.025 ± 0.003	−0.06 ± 0.03	0.18 ± 0.06	0.5 ± 0.3
Vertical export due to fertilization (vertical export minus background export)	24–36	0.40 ± 0.08	−0.012 ± 0.005	ND	0.1 ± 0.1	1.2 ± 0.4

Budgets were calculated for the surface layer (0–100 m) starting immediately after fertilization (day 0) and lasting until the last station where nutrients were measured inside the fertilized patch (day 36) (see Supplementary Methods for details). Total N includes $NO_2 + NO_3$, DON and ammonium. All values are in moles per square metre. Uncertainties (s.e.m.) were estimated by propagation of standard errors based on linear uptake models (Fig. 3) and measurement uncertainties. ND, not determined.
* Vertical export between days 0 and 24 (0.4 mol C m^{-2}; Supplementary Table 3) extrapolated to days 0–36 (Supplementary Methods).

barite[16] indicate that only ~11% of POC exported during the flux event was remineralized between depths of 200 and 1,000 m. By contrast, the background export until day 24 was largely respired above 500 m, because the POC increase below 200 m (Fig. 4) amounted to 0.04 mol C m^{-2}, which is <10% of the concomitant loss from the surface layer calculated from corrected element budgets. Identical rates of POC increase in subsurface layers outside the patch also indicate that background export was remineralized above 500 m.

We attribute the comparatively high POC stocks in outside waters (0.5 ± 0.1 mol C m^{-2} (s.d.) above background) between 200 and 1,000 m on day 5 and between 300 and 3,000 m on days 33 and 34 (Fig. 4) to slower sinking particle flux from the patchy natural blooms mentioned above (Supplementary Information). Local patchiness in out-stations is indicated by greater scatter in values from successive profiles taken during the same station than in in-stations (Figs 4 and 5).

The steep increase in POC stocks below 200 m under the patch after day 28 (Fig. 4) can be attributed to POC in the mucilaginous matrix of diatom aggregates in the >1-mm size range, which appeared as spikes in the transmissometer profiles. The occurrence of large aggregates reflected in spikiness of the profiles was notably higher under the hot spot than outside it (Supplementary Fig. 6). Sinking rates of >500 m d^{-1} and aggregates in the centimetre size range are required to account for the similar slopes of increasing POC at all depths down to the sea floor after day 28, just four days after the enhanced appearance of spikes (aggregate formation) at the pycnocline (Supplementary Fig. 6a) and visual observation of mass mortality in a major, spiny diatom species, *Chaetoceros dichaeta*. By contrast, the smaller aggregates from the less dense natural blooms sank more slowly than those from the patch. Coagulation models[19,20] of aggregate formation confirm the relationships between sinking rate and bloom density and, respectively, cell size (including spine length). The latter depends on the species composition of the bloom, which thus has a decisive role in the long-term fate of its biomass.

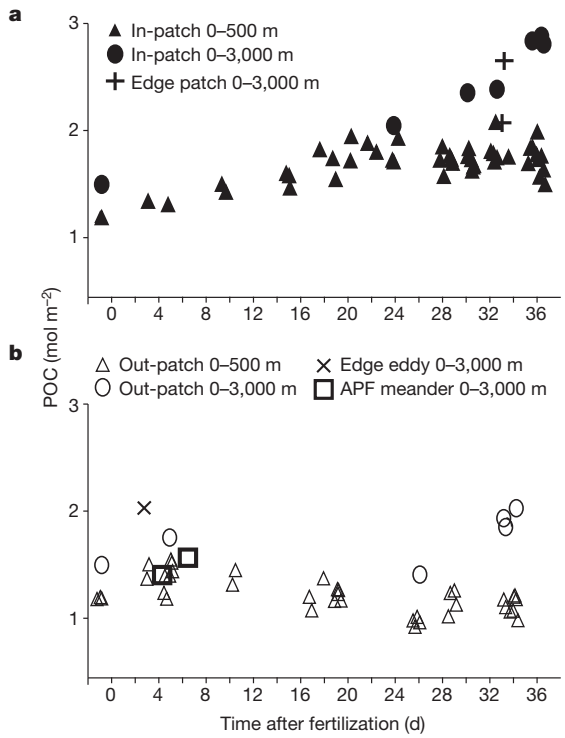

Figure 5 | Depth-integrated particulate organic carbon stocks. Stocks for the 0–500-m (triangles) and 0–3,000-m (circles) water columns are derived from vertical transmissometer profiles as in Fig. 4. Filled and open symbols show data inside and outside the patch, respectively. All profiles measured down to the sea floor during the study are depicted. Because the depth of the flux event was not anticipated and deep casts are time consuming, only six profiles to the sea floor were measured before the flux event: one before fertilization, one in the hot spot, two outside the patch (of which one was inside the core) and two in the meander of the Antarctic polar front (APF).

Organism stocks and rates

Biomass estimates from organism counts were highly correlated with the respective bulk measurements: the ratio of POC to phytoplankton carbon was 1.4 mol mol^{-1} ($r^2 = 0.54$, $P < 0.0001$), that of phytoplankton carbon to Chl was 27 mg mg^{-1} ($r^2 = 0.87$, $P < 0.0001$) and that of BSi to total diatom carbon was 0.9 mol mol^{-1} ($r^2 = 0.76$, $P < 0.0001$). This indicated that accumulation of particulate organic detritus was minor, that POC increments had a high cellular chlorophyll content as a result of newly accumulated biomass (POC/Chl = 32 mg mg^{-1}, $r^2 = 0.394$, $P < 0.0001$) and that new biomass was dominated by diatoms. Rates of primary production doubled following fertilization and stabilized at 0.13 mol C m^{-2} d^{-1} (1.5 ± 0.1 g C m^{-2} d^{-1}) from days 9 to 35 but declined to 0.08 mol C m^{-2} d^{-1} on day 36. The total C accumulation and export rates estimated from element budgets are easily accommodated in the organic carbon produced during the bloom (4.2 mol C m^{-2}, or 51 g C m^{-2}). The remainder could be attributed to recycling in the surface layer by bacteria, microzooplankton and copepods, whereby grazing pressure on the diatoms was lower than on other protists. Bacterial stocks and production rates declined by ~30% in the demise phase of the bloom, which supports the high transfer efficiency of POC to depth. Thus, the budgets of biological rates are remarkably consistent with other budgets.

In outside water, primary production amounted to 1.36 mol C m^{-2} (16 g C m^{-2}) over 34 days, which is too low to accommodate the estimated sinking losses of 1.2 mol C m^{-2} (14.4 g C m^{-2}; Supplementary Table 3) because bacterial remineralization rates and copepod grazing pressure were in the same range outside the patch as inside. The

discrepancy between measured production and estimated loss rates is partly due to three out-stations placed where there had been previous natural blooms with comparatively low surface DIC inventories (Fig. 3a) but where much of the corresponding POC stocks had already sunk to subsurface layers. Furthermore, the vertical diffusion coefficient applied[14] seems to lead to an overestimation of export. Applying another, twofold-higher, diffusion coefficient for diapycnal mixing derived from microstructure profiles during EIFEX[15] results in twofold-higher export values that are supported even less by direct observations of the plankton community and by POC profiles.

Conclusions

The peak chlorophyll stock of 286 mg m^{-2} is the highest recorded in an OIF experiment so far[5] and demonstrates that, contrary to the current view[21], a massive bloom can develop in a mixed layer as deep as 100 m. The EIFEX results provide support for the second condition of the iron hypothesis[4], that mass sinking of aggregated cells and chains in the demise phase of diatom blooms also occurs in the open Southern Ocean, both in natural[22,23] and in artificially fertilized blooms. Given the large sizes, high sinking rates and low respiratory losses of aggregates from the iron-induced bloom, much of the biomass is likely to have been deposited on the sea floor as a fluff layer[24] with carbon sequestration times of many centuries and longer. Larger-scale, longer-term OIF experiments will be required to reduce the effects of horizontal dilution and to explore further the potential of this technique for hypothesis testing in the fields of ecology, biogeochemistry and climate.

METHODS SUMMARY

The eddy was selected on the basis of satellite altimetry and surface chlorophyll distribution. Fertilization was carried out by releasing 7 t of commercial Fe(II) sulphate dissolved in 54 m^3 of acidified (HCl) sea water into the ship's propeller wash while spiralling out from a drifting buoy at 0.9-km radial intervals. By day 14, the initial 167-km^2 patch had spread and an area of 740 km^2 was again fertilized with 7 t of Fe(II) sulphate, this time along east–west transects 3 km apart, from north to south in the direction of the moving patch (Fig. 1c).

The patch was located using the drifting buoy, and the photochemical efficiency (F_v/F_m) was measured continuously with a fast-repetition-rate fluorometer. As in previous experiments, F_v/F_m was significantly higher in iron-fertilized water. Within a week, the bloom had accumulated sufficient biomass that additional tracers (chlorophyll concentration and continuous measurements of fCO_2) could be used to locate the part of the patch least affected by dilution with outside water, that is, that with the highest chlorophyll concentration and, in the last week, the lowest fCO_2 value (Fig. 1c–f). All in-stations were placed inside this hot spot and care was taken to locate it with small-scale surveys before sampling and to keep the ship within it during sampling at each station, which generally lasted about 8 h. Some in-stations were within the patch but were subsequently shown to have missed the hot spot and have therefore been excluded. For logistical reasons, the out-stations were taken in different locations of the core relative to the direction of the moving patch, that is, ahead, behind or diagonally opposite it.

Standard oceanographic methods and instruments[15] were used to collect samples and measure the properties of the water column. See Supplementary Information for details.

Received 15 November 2011; accepted 3 May 2012.

1. Sigman, D. M. Hain, M. P. & Haug, G. H. The polar ocean and glacial cycles in atmospheric CO_2 concentration. *Nature* **466,** 47–55 (2010).
2. Anderson, R. F. *et al.* Wind-driven upwelling in the Southern Ocean and the deglacial rise in atmospheric CO_2. *Science* **323,** 1443–1448 (2009).
3. Martin, J. H. Glacial-interglacial CO_2 changes: the iron hypothesis. *Paleoceanography* **5,** 1–13 (1990).
4. Coale, K. H. *et al.* Southern Ocean iron enrichment experiment: carbon cycling in high- and low-Si waters. *Science* **304,** 408–414 (2004).
5. Boyd, P. *et al.* Mesoscale iron-enrichment experiments 1993–2005: synthesis and future directions. *Science* **315,** 612–617 (2007).
6. Cassar, N. *et al.* The Southern Ocean biological response to aeolian iron deposition. *Science* **317,** 1067–1070 (2007).
7. Hamme, R. C. *et al.* Volcanic ash fuels anomalous plankton bloom in subarctic northeast Pacific. *Geophys. Res. Lett.* **37,** L19604 (2010).
8. Lampitt, R. S. *et al.* Material supply to the abyssal seafloor in the Northeast Atlantic. *Prog. Oceanogr.* **50,** 27–63 (2001).
9. Abelmann, A., Gersonde, R., Cortese, G., Kuhn, G. & Smetacek, V. Extensive phytoplankton blooms in the Atlantic sector of the glacial Southern Ocean. *Paleoceanography* **21,** PA1013 (2006).
10. Kohfeld, K. E., Le Quéré, C., Harrison, S. P. & Anderson, R. F. Role of marine biology in glacial-interglacial CO_2 cycles. *Science* **308,** 74–78 (2005).
11. The Royal Society. *Geoengineering the Climate: Science, Governance and Uncertainty*. RS policy document 10/09 (The Royal Society, 2009).
12. Chelton, D. B., Schlax, M. G., Samelson, R. M. & de Szoeke, R. A. Global observations of large oceanic eddies. *Geophys. Res. Lett.* **34,** L15606 (2007).
13. d'Ovidio, F., Isern-Fontanet, J., Lopez, C., Hernandez-Garcia, E. & Garcia-Ladona, E. Comparison between Eulerian diagnostics and finite-size Lyapunov exponents computed from altimetry in the Algerian basin. *Deep Sea Res. Part I Oceanogr. Res. Pap.* **56,** 15–31 (2009).
14. Hibbert, A., Leach, H., Strass, V. & Cisewski, B. Mixing in cyclonic eddies in the Antarctic Circumpolar Current. *J. Mar. Res.* **67,** 1–23 (2009).
15. Cisewski, B., Strass, V. H., Losch, M. & Prandke, H. Mixed layer analysis of a mesoscale eddy in the Antarctic Polar Front Zone. *J. Geophys. Res.* **113,** C05017 (2008).
16. Jacquet, S. H. M., Savoye, N., Dehairs, F., Strass, V. H. & Cardinal, D. D. Mesopelagic carbon remineralization during the European Iron Fertilization Experiment. *Glob. Biogeochem. Cycles* **22,** GB1023 (2008).
17. Paytan, A. & McLaughlin, K. The oceanic phosphorus cycle. *Chem. Rev.* **107,** 563–576 (2007).
18. Bishop, J. K. B., Wood, T. J., Davis, R. E. & Sherman, J. T. Robotic observations of enhanced carbon biomass and export at 55° S during SOFeX. *Science* **304,** 417–420 (2004).
19. Jackson, G. A. A model of the formation of marine algal flocs by physical coagulation processes. *Deep-Sea Res.* **37,** 1197–1211 (1990).
20. Riebesell, U. & Wolf-Gladrow, D. A. The relationship between physical aggregation of phytoplankton and particle flux: a numerical model. *Deep-Sea Res. A* **39,** 1085–1102 (1992).
21. de Baar, H. J. W. *et al.* Synthesis of iron fertilization experiments: from the iron age in the age of enlightenment. *J. Geophys. Res.* **110,** C09S16 (2005).
22. Blain, S. *et al.* Effect of natural iron fertilization on carbon sequestration in the Southern Ocean. *Nature* **446,** 1070–1074 (2007).
23. Pollard, R. *et al.* Southern Ocean deep-water carbon export enhanced by natural iron fertilization. *Nature* **457,** 577–580 (2009).
24. Beaulieu, S. E. in *Oceanography and Marine Biology. An Annual Review* (eds Gibson, R. N., Barnes, M. & Atkinson, R. J.) 171–232 (Taylor & Francis, 2002).

Supplementary Information is linked to the online version of the paper at www.nature.com/nature.

Acknowledgements We thank C. Balt, K. Loquay, S. Mkatshwa, H. Prandke, H. Rohr, M. Thomas and I. Vöge for help on board. We are also grateful to U. Struck for POC and PON analyses. The altimeter products were produced by Ssalto/Duacs and distributed by Aviso with support from Cnes. We thank the captain and crew of RV *Polarstern* (cruise ANT XXI/3) for support throughout the cruise.

Author Contributions V.S. and C.K. wrote the manuscript. V.S. directed the experiment and C.K. carried out the budget calculations. V.H.S., P.A., M.M. and D.W.-G. contributed to the preparation of the manuscript. V.H.S., B.C., H.L. and M.L. contributed physical data on mixed-layer depth dynamics, eddy coherence, patch movement and transmissometer data. N.S. provided thorium data. A.W. provided nutrient data. P.A. and J.H. provided phytoplankton and BSi data. F.D. carried out the Lagrangian analysis based on delayed-time altimetry. J.M.A. and G.J.H. provided bacterial data. C.N. and R.B. provided inorganic carbon data. G.M.B., C.K. and M.M.M. provided POC and PON data. P.C. provided the iron data. S.G. and A.T. provided DOM data. I.P. and L.J.H. performed the ^{14}C primary production measurements and provided high-pressure liquid chromatography data. R.R. provided data on photochemical efficiency (F_v/F_m). C.K., M.M.S. and A.T. provided Chl data. U.B., E.S., O.S. and J.S. provided data on the eddy core from a subsequent cruise and satellite Chl images.

Author Information Reprints and permissions information is available at www.nature.com/reprints. The authors declare no competing financial interests. Readers are welcome to comment on the online version of this article at www.nature.com/nature. Correspondence and requests for materials should be addressed to V.S. (victor.smetacek@awi.de) or C.K. (christine.klaas@awi.de).

doi:10.1038/nature11229

Supplementary information

Table of contents

Supplementary Information SI 1
Properties of the eddy core and surrounding frontal meander

The eddy core and the surrounding Antarctic Polar Front (APF) meander were mapped and the distributions of physical, chemical and biological properties measured during a quasi-synoptic survey with a grid of 80 stations along 8 north/south transects 22 km apart from days 1 – 7, i.e. shortly after the patch was fertilized on day 0. The ADCP derived stream function and altimeter image from this survey are shown in Fig. 1 a and b (main text). The corresponding nutrient, chlorophyll and diatom carbon distributions are shown in Fig. S1.1. Each station in the grid (Fig. S1.1 c) consisted of a single CTD cast to 500 m depth which provided vertical profiles of temperature, salinity, chlorophyll fluorescence and beam attenuation of the transmissometer. Surface samples from the ship's seawater intake were taken for measurements of nutrients, chlorophyll *a* and microplankton composition and biomass along the survey (Fig. S1.1 b and e). Integrated POC stocks recorded with the profiling transmissometer are depicted for the upper 500 m and for each of the layers 0-100, 100-200, 200-300, 300-400, 400-500 m separately in Fig. S1.2. The grid was interrupted on days 4 and 5 for one full in and two out stations, respectively.

Values for all parameters (fig. S1.1) are consistently higher in the closed eddy core and the duct connecting it with Antarctic Zone (AZ) water in the south-eastern corner of the grid than in the surrounding APF meander. The closed core and its origin from the AZ are clearly represented in the high silicate and nitrate concentrations (Fig. S1.1 a-b). Note the larger gradient in silicate compared to nitrate from core centre to the surrounding meander of the APF. Phosphate distribution within the core is patchier than Si and N but nevertheless distinctly higher than in the meander (Fig. S1.1 c).

The same chlorophyll values, but depicted at different scales, are shown in panels d and f of Fig. S1.1. In panel d the same scale as in Fig. 1 c and f of the main text has been used to highlight the concentrations reached in the iron-induced bloom (see Fig. 1 c, f main text). The chlorophyll scale used in panel e encompasses the measured values in order to magnify variability in horizontal distribution. The orange region marked with the oval in the upper part of panel e is the patch, crossed on grid transects 3 and 4 (from West to East), on days 3 and 4 after fertilization. The apparent patch elongation is a sampling artefact as the patch was moving eastward with the survey. Distribution of total diatom biomass (determined from surface samples counted under the microscope) shown in panel f also exhibits horizontal variability which does not quite match that of chlorophyll presumably due to differences in C/Chl ratios between iron-starved and iron-replete cells and shifts in the ratio of total phytoplankton (i.e. including autotrophic flagellates) to diatom carbon biomass (~ 1 in that period). Whereas the range of concentrations of chlorophyll and diatom carbon within the eddy core is only twofold, the range of these values across the entire eddy is about sixfold.

The scales used to depict integrated POC stocks in different layers shown in Fig. S1.2 span the same range as the respective depth layers in Fig. 4 of the main text. Thus, maximum POC stocks recorded in the patch would appear deep red in all these figures. The greater horizontal homogeneity of POC stocks compared to values for Chl and diatom biomass can be explained by variability in C/Chl ratios leading to a much smaller POC increment of the growing bloom relative to background values and the fact that the former is an integrated value for the 100 m water column, whereas the latter are surface values. Since the survey was carried out in a period of relatively calm weather, accumulation of phytoplankton biomass in the surface could have led to the discrepancy. Further, diatom C at the start of the experiment accounted for only 28% of total POC.

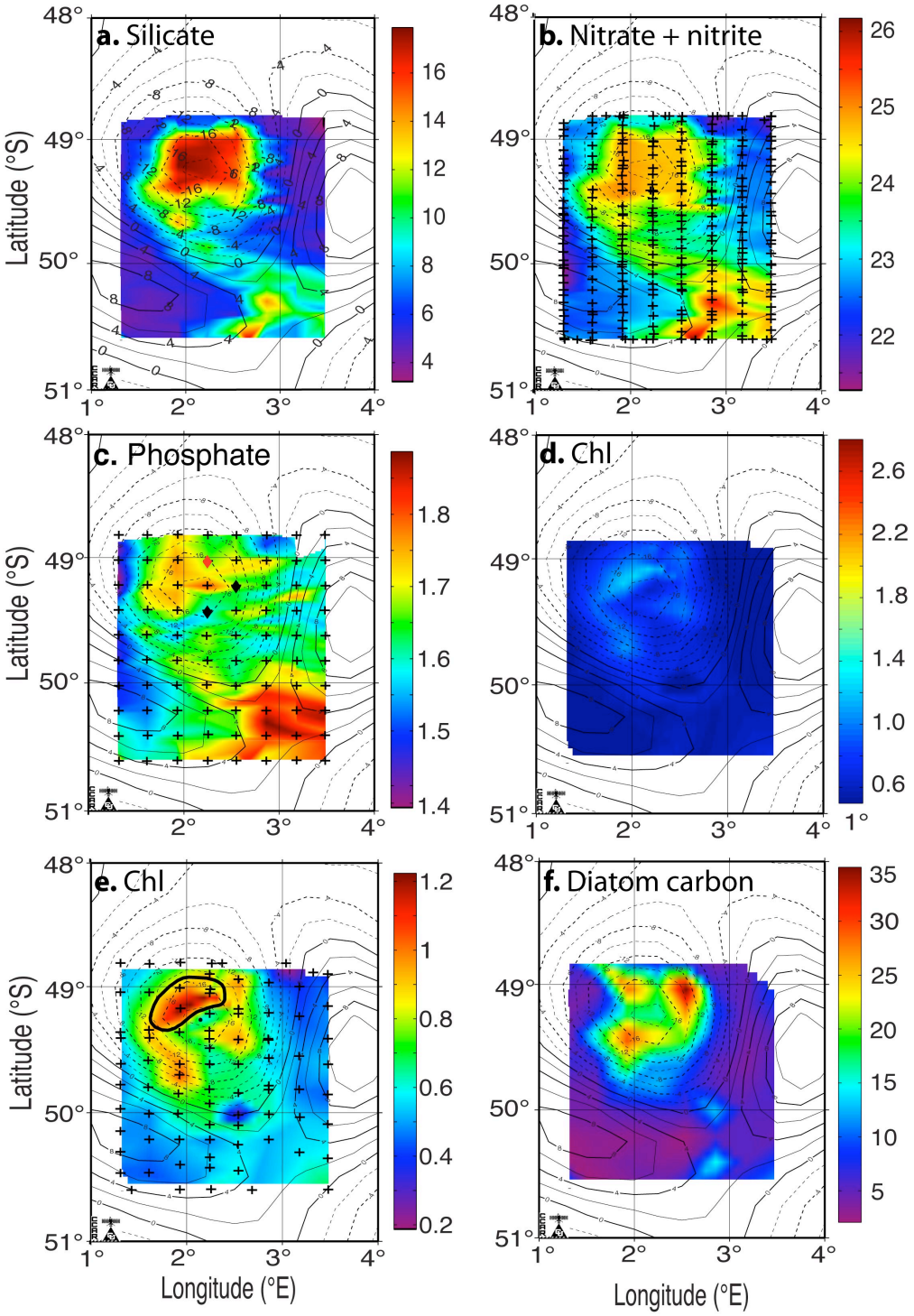

Fig. S1.1. Nutrient, chlorophyll *a* (Chl) and diatom biomass distribution during the eddy survey carried out from day 1 to day 7 after fertilization (14th to 20th February 2004). Nutrients in mmol m^{-3}, Chl and diatom carbon in mg m^{-3}. Crosses in panel c show location of CTD stations. The grid was interrupted on days 4 and 5 for one full in-station (red diamond in panel c) and two out-stations (black diamonds in panel c), respectively. Location of surface underway measurements are shown as crosses in panel b (all nutrients) and e (chlorophyll). The approximate location of the patch is marked with an elongated oval in panel e. Note minor, natural blooms to the east and south of the EIFEX patch. The surface chlorophyll distribution on panel d is given, for comparison, using the same colour-scale as in the Figure 1 c – f (main text). Background isopleths correspond to sea surface height anomalies (in cm) from February 18th 2004 obtained from the Near-Real-Time Altimetry Project, Colorado Center for Astrodynamics Research (CCAR), http://argo.colorado.edu/~realtime/gsfc_global-real-time_ssh/

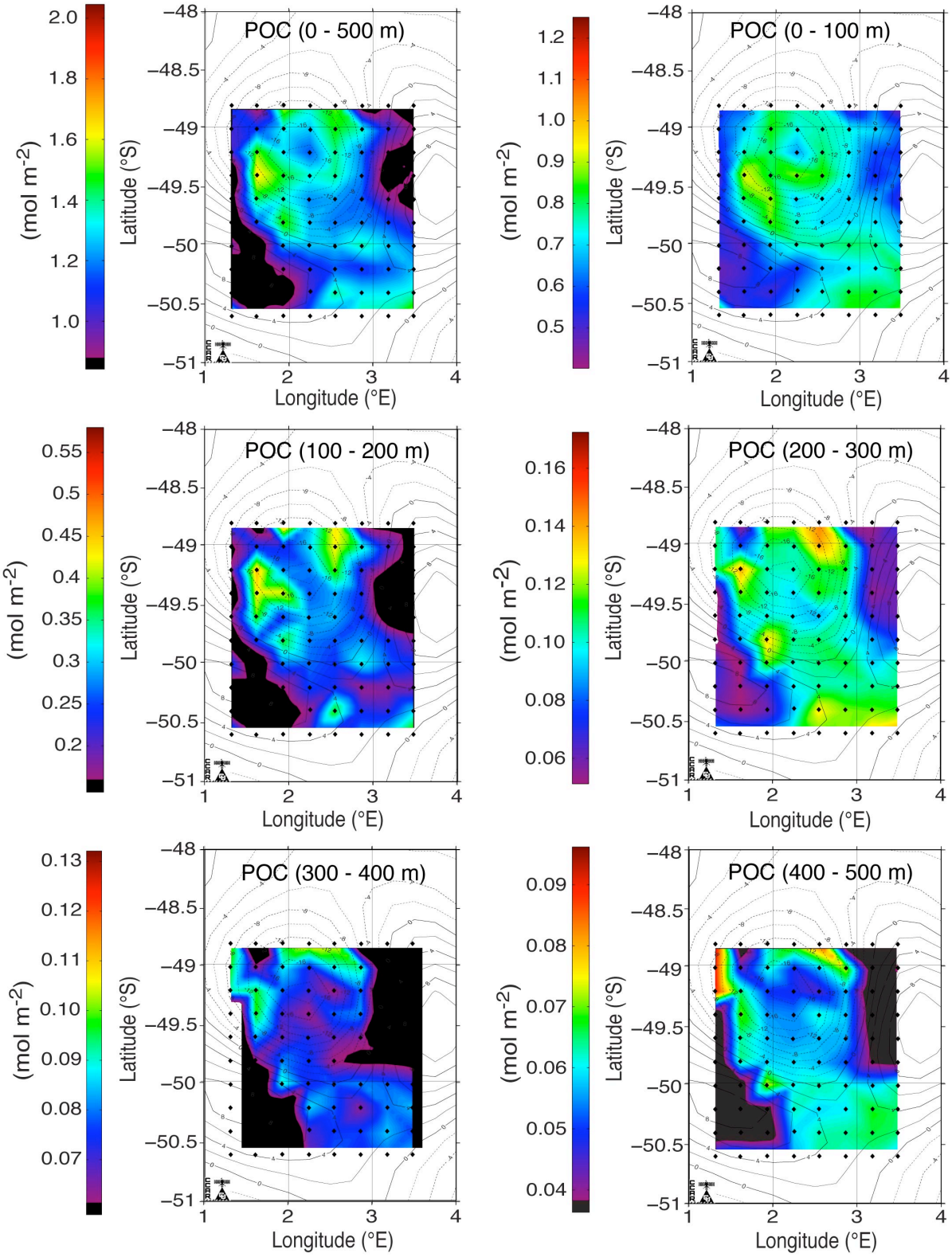

Fig. S1.2. Integrated particulate organic carbon stock distribution in the closed core and APF meander recorded during the same grid as Fig. 1 and S1.1. Upper left panel shows stocks for the layer integrated over 0 – 500 m and the other panels show integrated stocks for successive 100 m layers as indicated. POC stocks are derived from beam attenuation of a profiling transmissometer mounted on a CTD rosette calibrated with discrete POC measurements (Supplementary Figure 5). Positions of CTD casts are indicated by the black diamonds. For comparison, the colour scales span the same range in POC stock as the Y scales in Fig. 4 (main text) for the corresponding depth intervals. Black background indicates values smaller than minimum values of corresponding range in Fig. 4. Background isopleths are the same as in Fig. S1.1.

POC stocks integrated to 500 m depth within the eddy core ranged between 1.2 and 1.5 mol C m^{-2} and exhibited a greater degree of patchiness than in the surface layer due to variability in stocks in the deeper layers. The lowest subsurface POC stocks in the core were found in the region in which the patch was located. This region extended to the centre of the core with higher values "ahead" but particularly "behind" the patch in the direction of flow. Since the locations of out-stations relative to the patch were selected for logistical reasons, they were sometimes inadvertently located in these regions of higher POC stocks. Thus, during the first survey out stations had higher particulate stocks than the station on day -1 and the in-station on day 4.

We attribute the higher POC stocks in deeper layers to ongoing particle flux from the surface which was remarkably patchy at local scales. This is indicated by the wide range of POC stocks in the upper 500 m measured by successive casts taken several hours apart during the out-station on day 5 which was located in a region of higher diatom biomass in the surface (Fig. 4 k-n, main text). The only deep cast taken at this station happened to be one with higher deep particle stocks than most of the other casts. The higher values extended only to 1,000 m depth, stocks below 1,000 m were similar to pre-fertilization deep stocks (Fig. 4 o-p, main text). Higher POC stocks were again encountered in deeper layers during the last out-stations on days 33-34. High values now extended down to 3,000 m depth, concomitant with a decline above 300 m depth compared to stocks from day 5 (Fig. 4, main text) suggestive of sinking rates in the order of 10 - 100 m d^{-1} in the intervening period. These higher stocks were absent in the previous deep cast of the out-station taken on day 25 which was evidently located in the region of low POC stocks, hence comparable to the initial conditions of the fertilized patch and representative of most of the out-stations (Fig. 4, main text). The tenfold higher sinking speeds of aggregates from the patch could be explained by their larger size (compare profiles in Supplementary Fig. 6 c with d).

The patchy higher POC stocks in deep layers of the core outside the patch (Fig. S1.2.) are most probably due to the effects of local differences in iron input by aeolian dust. The difference between the lowest and highest out-station POC stocks between 0 – 3,000 m on days 25 and 34 respectively is 0.62 mol C m^{-2}. The maximum biomass attained by these natural blooms was less than half that attained in the hotspot. For comparison, the average value present in the upper 500 m of the hotspot from day 20 – 36 was 1.7 ± 0.1 mol C m^{-2} (n = 34) and the maximum values for the 0 - 3000 m water column on day 36 were 2.84 ± 0.04 mol C m^{-2} (n=3).

In striking contrast to the eddy core, POC stocks in the surrounding APF meander recorded during the grid in the upper 500 m were consistently < 1.0 mol C m^{-2}. The 2 deep casts taken in the meander (1.4 and 1.6 mol C m^{-2} between 0 – 3,000 m) were in the same range as the lower values from days -1 and 25 out-patch (Fig. 5 main text). The higher 0 – 3,000 m value of 2.1 mol C m^{-2} obtained on day 3 was from a station located in the outer rim of the eddy and was similar to the maximum out-patch values taken on day 35. The low POC stocks in the deep water column of the meander are of particular interest as satellite images show that it had been the site of a bloom 2 weeks prior to our arrival (Fig. 1 g, main text). This extensive bloom along the APF had presumably been terminated by a combination of iron and silicate limitation. Hence, the low POC stocks indicate that biomass built up in the bloom had settled out of the water column within a two-week period. The transmissometer profile recorded in the centre of the eddy 50 days after fertilization during a following cruise (ANT XXI/4) indicated a lower particle load than during EIFEX. The profile could not be accurately converted into POC because instrument drift in the interim was not accounted for,. High uptake rates of oxygen across the sediment/water interface were measured with a bottom lander equipped with an array of O_2 sensors under the APF meander southwest of the core during ANT XXI/4. These measurements indicated that a substantial amount

of POC had been previously deposited on the sea floor. Similar O_2 uptake rates were found at the sediment surface under the eddy core which we assume resulted from deposition of POC from the iron-induced bloom. In contrast, O_2 uptake rates recorded at a site in the AZ further to the south were threefold lower.

Conclusions

a) The water mass comprising the closed core of the eddy originated from the AZ south of the APF.
b) Most properties within the core varied by <30%, indicating a coherent water mass of the same provenance within the core.
c) However, chlorophyll concentrations, diatom biomass and deep POC stocks varied by a factor of 2 within the core but outside the patch due to processes initiated after formation of the eddy.
d) POC from the patchy natural blooms sank deep but more slowly than from the iron-induced bloom.
e) The high POC stocks in the hotspot water column could only have come from the overlying iron-induced bloom.

Supplementary Information SI 2
Eddy dynamics and dilution

Lateral stirring and eddy dilution

Lateral stirring is able to induce filaments by which water is exchanged between the core and the exterior of eddies. This process strongly depends on the temporal variability of the velocity field and arises on spatiotemporal scales of the order of ~10-100 km and weeks/months - relevant for the duration and size of the fertilization. In order to minimize the dilution of the fertilized patch due to the lateral stirring, the eddy was chosen on the basis of two dynamical characteristics observed from altimetry before and during the cruise: (i) an extremely slow temporal variability and (ii) a very weak interaction with the other nearby eddies. These characteristics persisted during the cruise. In order to confirm quantitatively that these characteristics implied a weak dilution of the eddy core, we performed a post-cruise Lagrangian analysis based on altimetry data[1].

The analysis was based on the calculation of Okubo-Weiss parameter, finite-size Lyapunov exponent[2] and particle trajectories. These tools applied to altimetry have been shown to describe in a robust way the filamentation of mesoscale eddies by lateral stirring, reproducing filaments well matched in chlorophyll and sea surface temperature images[1,3,4].

The Okubo-Weiss parameter is routinely used to localize eddies from snapshots of the velocity field. This diagnostic provides the dominance of the strain rate in respect to vorticity and therefore marks with negative values regions occupied by eddies. Calling u and v respectively the longitudinal and zonal component of the velocities, one can measure the normal and shear components of the strain S_n and S_s and the vorticity ω:

$$S_s=\partial v/\partial x+\partial u/\partial y$$

$$S_n=\partial u/\partial x-\partial v/\partial y$$

$$\omega=\partial v/\partial x-\partial u/\partial y$$

Then the Okubo-Weiss parameter W is

$$W= S_n^2+S_s^2-\omega^2$$

The Lyapunov exponent is computed at point x and time t by calculating the separation of trajectories initialized nearby backward in time. This is achieved by integrating the altimetry-derived geostrophic velocities. Calling δ_0 and δ respectively the initial and final trajectories' separation and Δt the time needed to reach the separation δ, the local Lyapunov exponent λ is obtained by assuming an exponential separation of the nearby trajectories:

$$\delta = \delta_0 \exp(\lambda . \Delta t)$$

Inverting this relation one can find the Lyapunov exponent as:

$$\lambda (x,t)= (1/\Delta t) \log(\delta /\delta_0)$$

In physical terms, the value of the Lyapunov exponent indicates the exponential stretching that a parcel of water undergoes while it is advected. Maxima of Lyapunov exponents correspond to sharp

fronts of tracers that have been passively advected for timescales of the order of $1/\lambda$ (refs.1,3,5,6).

The combination of Okubo-Weiss and Lyapunov exponents has been shown to be a powerful tool for detecting the position of mesoscale eddies and the effect of these eddies on advected tracers[3]. Here we used this approach to identify the fertilized eddy and the fronts defining the boundaries of the eddy core. The analysis was based on geostrophic velocities produced by AVISO from satellite sea surface height anomalies[7] and RIO-05 mean dynamic topography[8] that were linearly interpolated in space and time when needed. Integration of the velocity was done with a Runge-Kutta integrator of fourth order. Details of the calculation can be found in refs. 2 and 3.

A map of Okubo-Weiss parameter and local Lyapunov exponent for the first day after fertilization (14 February 2004) is shown in Figs. S2.1 and S2.2, where a white square indicates the centre of the fertilized patch. The Okubo-Weiss map reveals the fertilized eddy as the dominant recirculating structure (in terms of vorticity vs. strain signature) in the mesoscale field. The lines of Lyapunov maximal values (corresponding to fronts that separate water masses of different origin) show this eddy as the one with the most regular and closed core. This difference is remarkable when the core of the fertilized eddy is compared to the core of the anticyclone at 3.7˚E, 49.2˚S which has a relatively strong Okubo-Weiss signature but lacks an isolated core, appearing in the Lyapunov map only as a lobe of the Antarctic Circumpolar Current. This is a consequence of both a stronger vorticity and weaker temporal dynamics of the fertilized eddy in comparison to the other eddies of the region. The fertilized eddy contains a core centered at 2.25˚E, 49.6˚S with a diameter of about 60 km, encircled by a peripheral region with a width of ~20 km. A meander of the Antarctic Circumpolar Current is visible around the eddy. The South-East sector of the core is shifted South-East in respect to the boundary detected by the Okubo-Weissparameter, otherwise the core is fairly aligned with Okubo-Weiss isolines. The core is characterized by a very weak stretching rate (Lyapunov exponents less than 0.1 d^{-1}) and is delimited by Lyapunov exponents in excess of 0.3 d^{-1}. We recall that the intensity of Lyapunov values indicate the timescale over which a tracer contour aligns to the line of maximal Lyapunov exponents[3]. For the case of the core boundaries, this corresponds to $1/0.3 \approx 3$ days. The core appears to exchange water only through a thin duct a few kilometers wide, stemming from the southern edge of the core and extending westward. This analysis is consistent with the numerical advection of a test tracer initially located inside the eddy at the day of fertilization (Fig. S2.3).

These results from delayed-time altimetry strongly support the pre- and in-cruise analysis based on near-real-time altimetry, confirming a weak perturbation of the fertilized eddy by the other eddies and an almost closed structure of the eddy core. Note also that the south-eastward shift of the Lagrangian core (i.e., of the water mass most isolated inside the eddy) relative to the position of the centre of the sea surface height anomaly (or Okubo-Weiss minimum) balanced the inadvertent off-centre error during the placement of the fertilized patch.

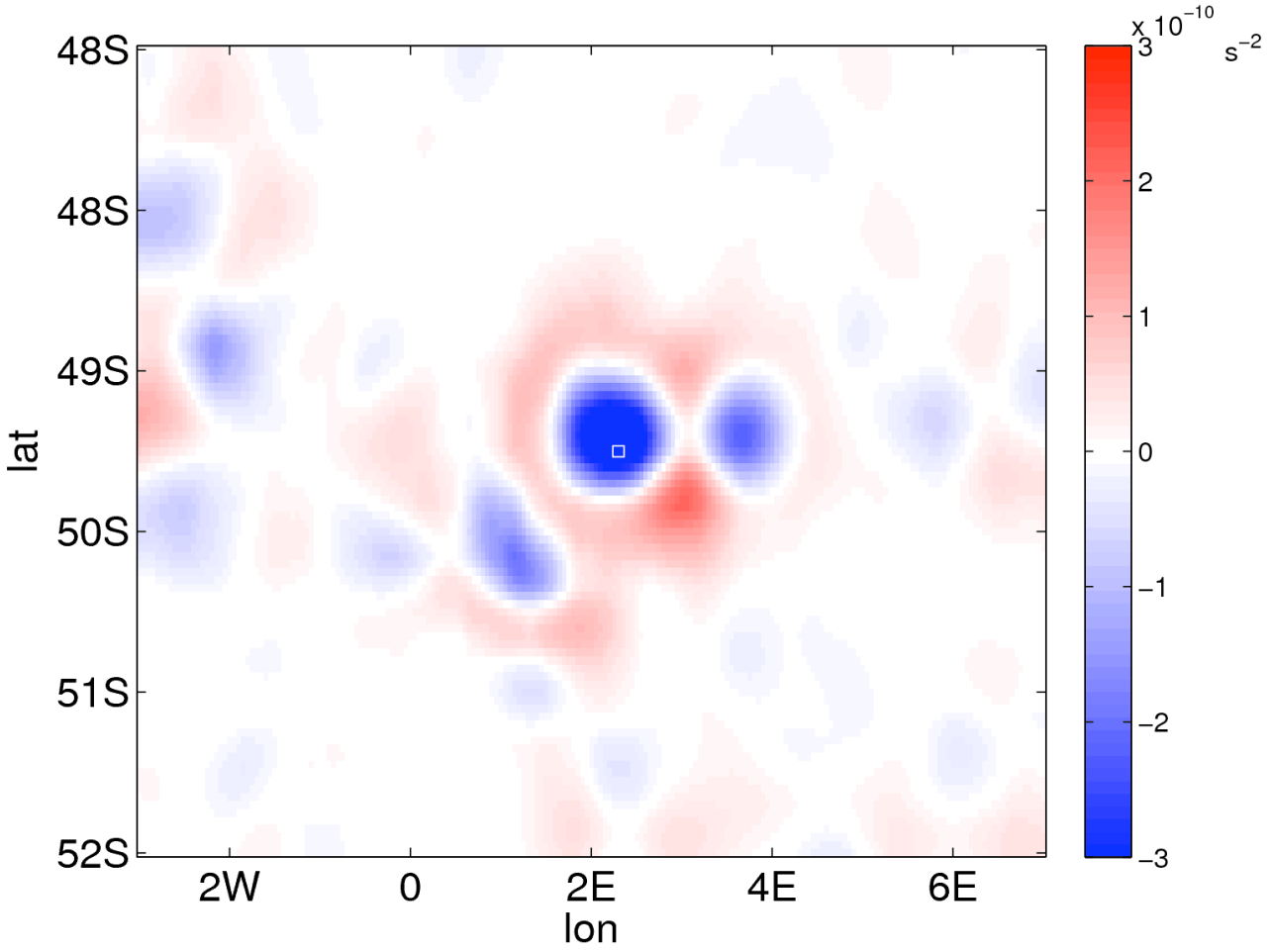

Figure S2.1. Eddy detection. Okubo-Weiss parameter calculated from altimetry-derived geostrophic velocity at the beginning of the experiment (14th February 2004). The Okubo-Weiss parameter identifies eddies as regions where vorticity dominates the strain rate. The white square corresponds to the centre of the fertilized patch.

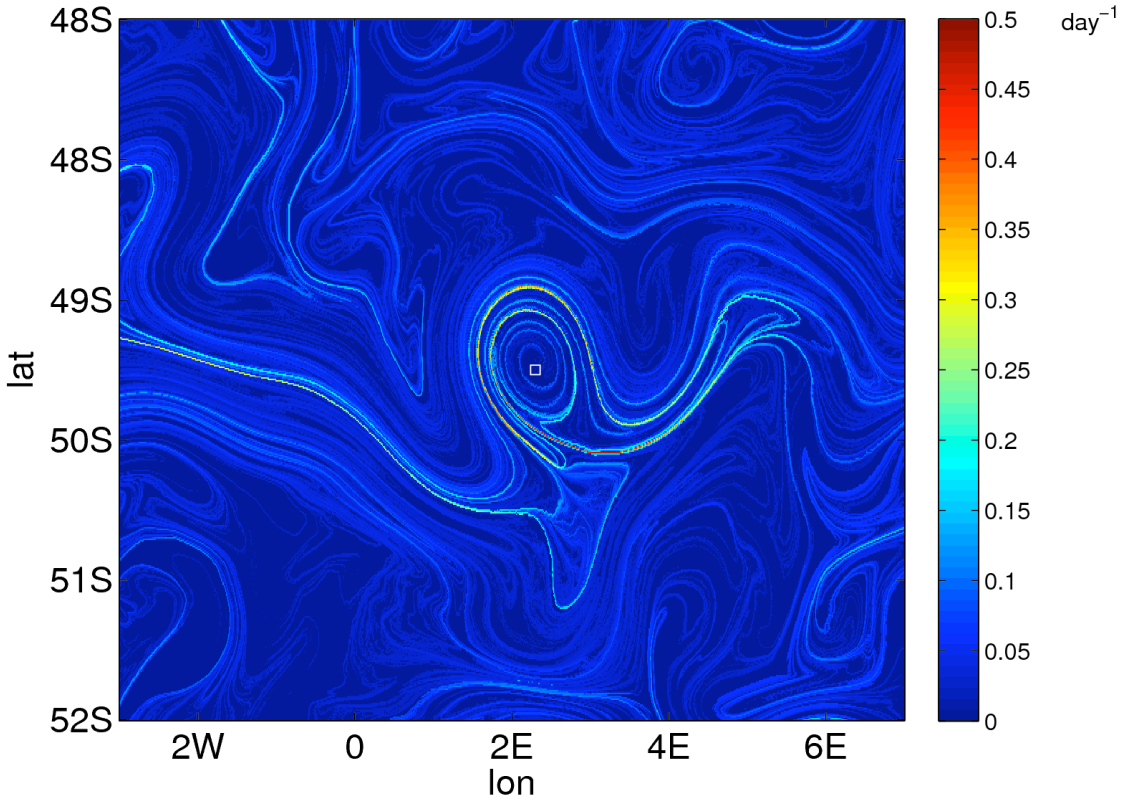

Figure S2.2. Fronts induced by lateral stirring. Lyapunov exponent calculated from altimetry-derived geostrophic velocity at the beginning of the experiment (14th February 2004). The Lyapunov exponent (d^{-1}) measures the stretching of an advected parcel of fluid. Lines of maxima of Lyapunov exponent indicate transport barriers induced by the lateral stirring. These lines can be interpreted as fronts between water masses of different origins (see text for an interpretation of the Lyapunov values). The white square corresponds to the centre of the fertilized patch. Note that the fertilized eddy is the only mesoscale structure in the region with a core well bounded by transport barriers.

Core dynamics and dilution rate

In order to quantify the dilution of the eddy core during the experiment, we reconstructed the evolution of the eddy content by numerically measuring the advection of a test tracer initially placed in the region of negative Okubo-Weiss values. The advection was done by integration of altimetry-derived geostrophic velocities, linearly interpolating in space and time when needed. The Okubo-Weiss signature of the eddy was tracked for each day. Some snapshots of the advected patch are shown in Fig. S2.3. By reconstructing the origin of the eddy content for each day, we estimated the dilution rate as the fraction of the initial eddy content that was exchanged[1]. The fraction of the tracer located inside the eddy at the day of fertilization and still present inside the eddy in the following days is plotted in Fig. S2.4. As expected by the eddy structure revealed by the Lyapunov analysis, there is a sharp decrease during the first days, when the content of the eddy periphery is rapidly ejected (8-10 days). This part of the eddy accounts for 20-25% of the original content of the eddy and corresponds equivalently to a dilution rate of 2-3%/day. The dilution proceeds then at a much slower speed (about 0.1%/day) when the content of the eddy core starts to be eroded. We thus

concluded that during the experiment (38 days) the eddy core may have been contaminated by the intrusion of surrounding waters by less than 10%.

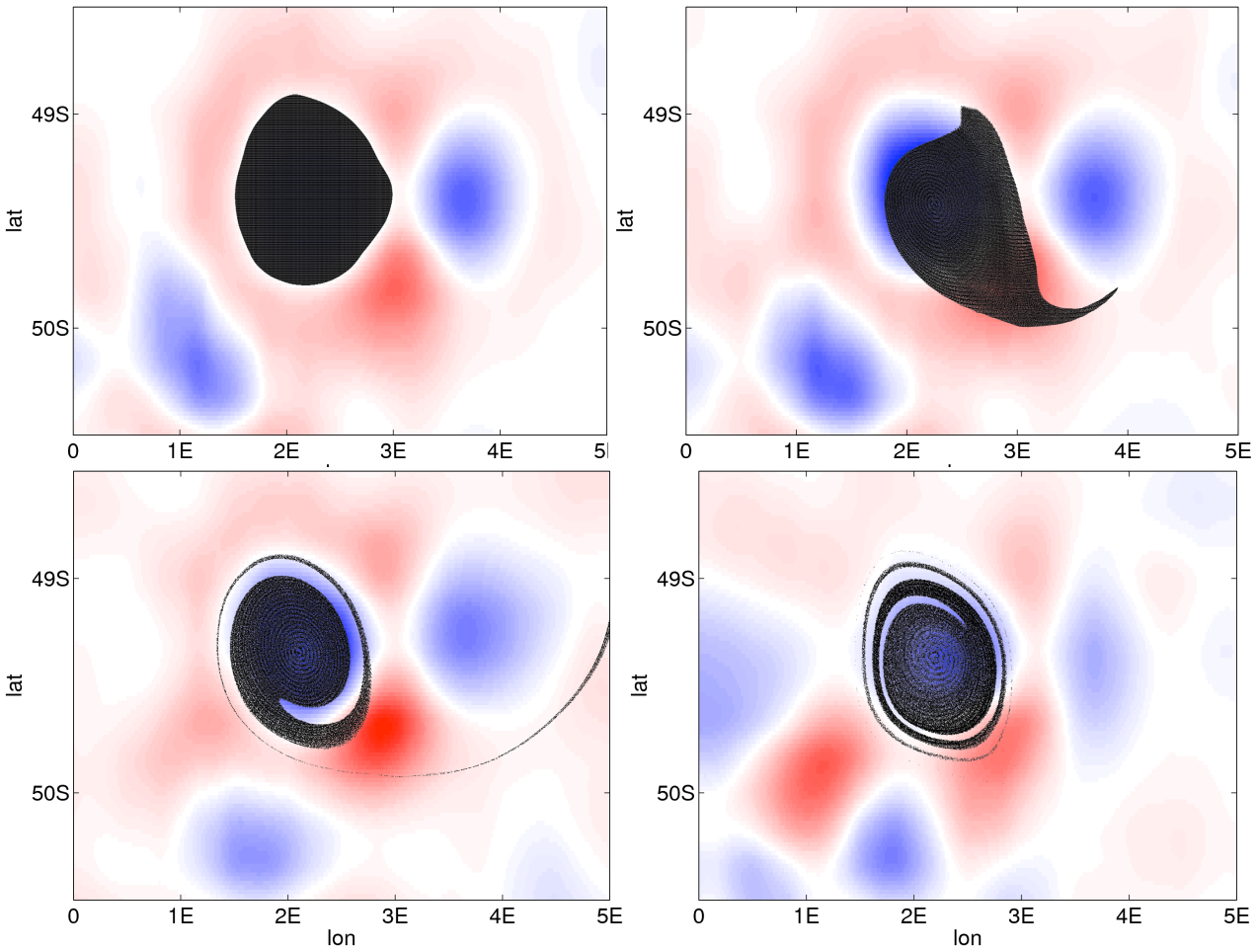

Figure S2.3. Lagrangian evolution of the eddy content. Advection of a numerical tracer (black dots) and Okubo-Weiss parameter (color scale as in Fig. S1.1).The tracer is initialized inside the fertilized eddy on the 13th of February 2004. The panels show the evolution of the tracer and the Okubo-Weiss field at day 0, 2, 8, and 16 from fertilization (i.e., February 13, 15, 21 and 1st of March 2004, from left to right and from top to bottom). Note that already at the second day most of the tracer contained in the eddy periphery is ejected. After eight days the tracer shadows the structure unveiled by the Lyapunov exponent analysis. After sixteen days the core is still mostly preserved, being only eroded by a very thin filament. Spatial structures and timescales are in excellent agreement with results from the Lyapunov analysis.

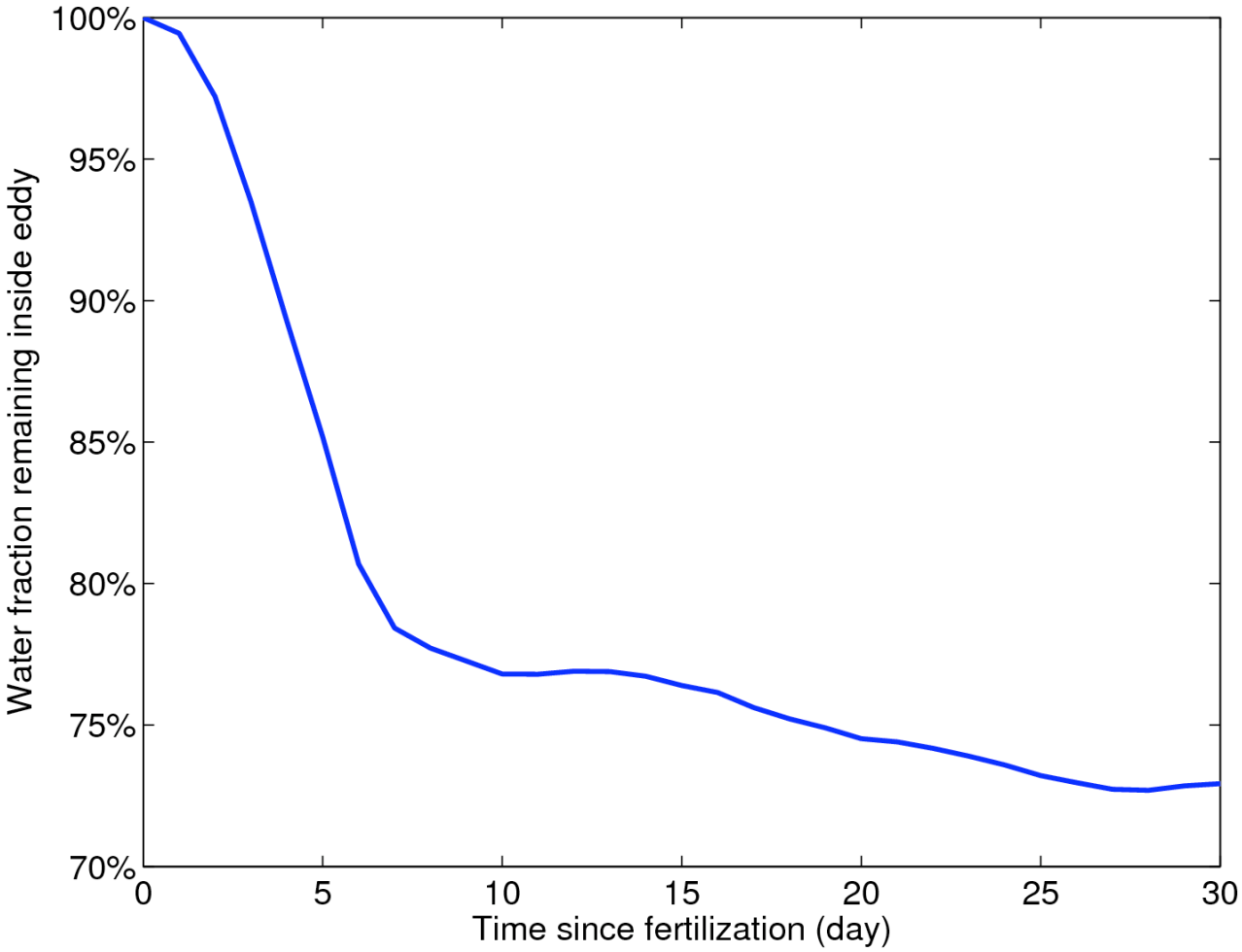

Figure S2.4. Eddy dilution. The plot shows the fraction of the original content of the EIFEX eddy (defined as the region with negative Okubo-Weiss) that remained inside the eddy as a function of time from 12th February 2004. The eddy region is defined as a circle of 100 km centered over the eddy centre (computed as the minimum of the Okubo-Weiss parameter at each day). In agreement with the Lyapunov analysis (Fig. S2.2) and particle trajectories (Fig. S2.3), the eddy dilution occurs in two steps: a fast ejection of the periphery (days 5-10, 20-25% of the eddy content) followed by a much slower erosion of the core (about 2-3% of the eddy, or 3-4% of the core, in 20 days).

References for SI 2

1. Lehahn, Y., d'Ovidio, F., Lévy, M. & Heifetz, E. Stirring of the northeast Atlantic spring bloom: A Lagrangian analysis based on multisatellite data. *J. of Geophys. Res.* **Vol 112**, C08005 (2007).

2. d'Ovidio, F., Fernandez, V., Hernandez-Garcia, E. & Lopez, C. Mixing structures in the Mediterranean Sea from finite-size Lyapunov exponents. *Geophys. Res. Lett.* **Vol 31** , L17203 (2004).

3. d'Ovidio, F., Isern-Fontanet, J., López, C., García-Ladona, E. & Hernández-García, E. Comparison between Eulerian diagnostics and the finite-size Lyapunov exponent computed from altimetry in the Algerian Basin. *Deep Sea Res. I* **56**, 15-31 (2009).

4. Beron-Vera, F. J., Olascoaga, M. J. & and Goni, G. J. Oceanic mesoscale eddies as revealed by Lagrangian coherent structures. *Geophys. Res. Lett.* **35**, L12603 (2008).

5. Boffetta, G., Lacorata, G., Redaelli, G. & Vulpiani, A. Detecting barriers of transport: a review of different techniques. *Physica D* **159**, 58-70 (2001).

6. Shadden, S.C., Lekien, F. & Marsden, J. E. Definition and properties of Lagrangian coherent structures from finite-time Lyapunov exponents in two-dimensional aperiodic flows. *Physica D* **212**, 271-304 (2005).

7. Ssalto/Duacs User handbook (M)SLA and (M)ADT near-real time and delayed time products. CLS-DOS-NT-06.034 (2006)

8. Rio, M.-H., Poulain, P.-M., Pascual, A., Mauri, E., Larnicol, G. & Santoleri, R. A Mean Dynamic Topography of the Mediterranean Sea computed from altimetric data, in-situ measurements and a general circulation model. *J. Mar. Sys.* **65**, 484-508 (2007).

Supplementary Information SI 3
Patch area evolution and dilution rates

Patch area
The patch areas were determined using data from the two complete surveys of the patch. Survey 1 was conducted between 23-24 February and survey 2, conducted on 1-3 March (Table S3.1). As criteria defining the fertilized patch (threshold values) we used Chl $\geq$ 1.2 mg m^{-3} (main text Fig. 1 c and 1 f), Fv/Fm $\geq$ 0.5 (main text Fig. 1 d) and fCO_2 $\leq$ 355 µatm (main text Fig. 1 e). Fv/Fm was measured continuously over the whole survey area only during survey 2. Patch area was calculated using threshold values after correction for displacement and distortion, which resulted from the flow field (using the ADCP-measured current vectors) and interpolation of the data on a regular mesh grid of 1 minute of latitude by 1 minute of longitude.

Table S3.1. Patch area.

Survey	Variable	Threshold value	Mean Survey Time [Days after fertilization]	Area [km²]	Average Area [km²]
0	Fe Fertilization		0	167	
1	Chl (mg m^{-3})	1.2	11.1	558	447
1	fCO_2 (µatm)	355	11.2	336	
2	Chl (mg m^{-3})	1.2	18.7	871	798
2	fCO_2 (µatm)	355	18.7	782	
2	Fv/Fm	0.5	18.7	741	

Because a complete Fv/Fm patch survey was only performed once and because the variables Chl and fCO_2 cannot be considered conservative, we have also employed a model study to assess the spreading of the patch during the course of the experiment.

Model of patch evolution
An optimal circulation model was obtained by fitting the circulation to observations of temperature, salinity, and velocities with variational state estimation techniques. The regional model is based on the MITgcm (http://mitgcm.org). It covers the experimental site with a grid spacing of approximately 3.6 km and 30 vertical layers spanning the top 500 m and has a state-of-the-art vertical mixed layer scheme and four open boundaries (Losch, M. et al. "Ocean state estimation from hydrography and velocity observations during EIFEX with a regional ocean circulation model", to be submitted). An idealized, perfectly passive tracer is released into this circulation over the course of day 0 of the simulation; the initial patch covered approximately the same area as the first EIFEX iron patch (within the accuracy set by the model grid resolution). To estimate the physical evolution of the patch following the method of Stanton et al. (1998), the first and second

moments (relative to the centre of mass) of the passive tracer distribution are calculated for every 4th hour of the model simulation. The squared mean radial distance of a tracer particle from the centre of mass is estimated from these moments under the assumption of a Gaussian distribution of the tracer concentrations as $m_2/m_0 - m_1^2/m_0^2$, where m_i is the i'th moment (Fig. S3.1). The assumption of a Gaussian distribution is, however, not valid for the first days of the integration when the patch concentration is nearly homogeneous and has a sharp edge.

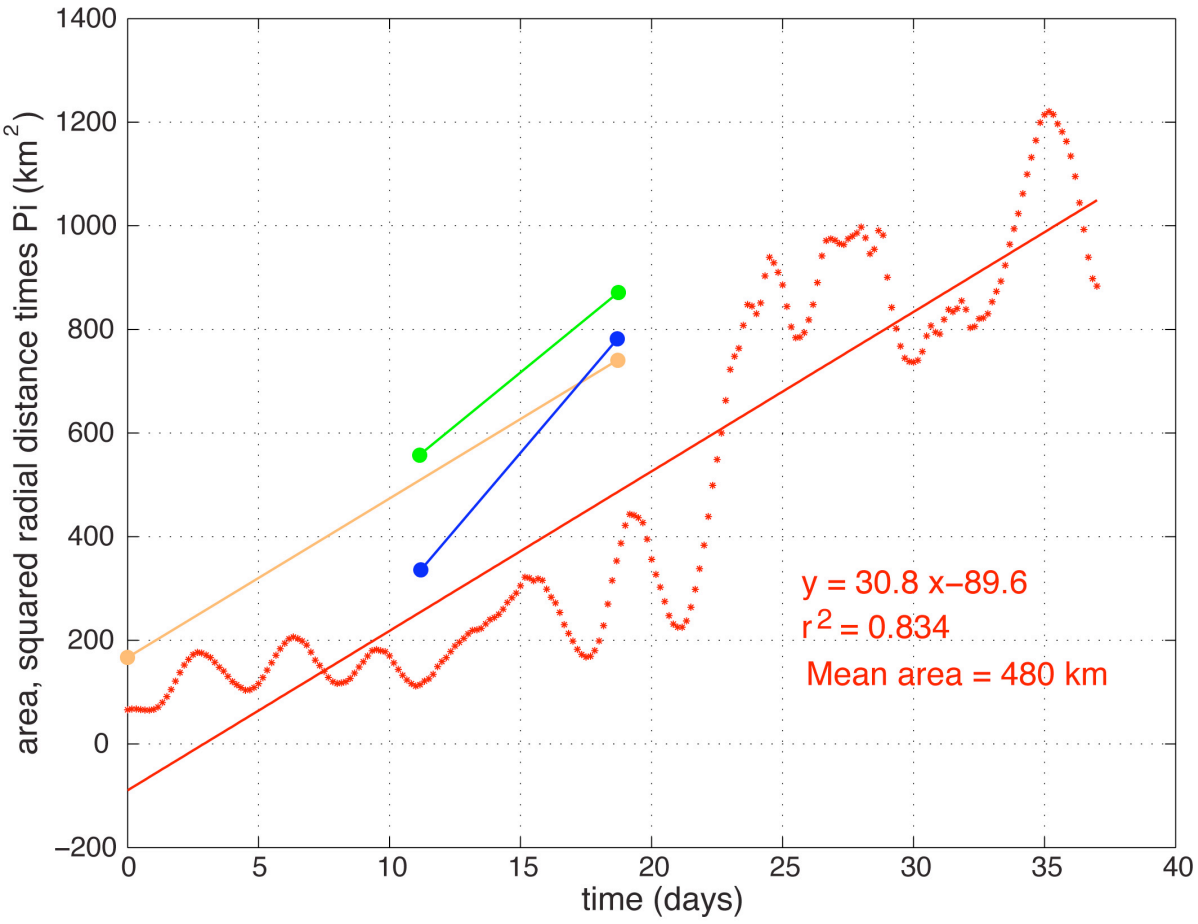

Figure S3.1. Temporal development of the patch area as estimated by the model-calculated squared radial distance multiplied by π (red dots) and patch areas obtained from the surveys of fCO_2 (blue dots), Fv/Fm (orange dots) and Chl (green dots). The different parameters used to define patch boundaries leads to the scatter in patch areas obtained at a given time, however, they have a minor effect on the estimation of temporal developments of the patch sizes.

Using the same model data for a regression of the squared radial distance versus time in seconds yields a slope of 113 which after division by 2 translates into a horizontal diffusivity of 56 $m^2 s^{-1}$.

Dilution rates

From the temporal evolution of the patch area (A) the dilution rate for the whole patch (γ) can be estimated by assuming that the patch area increases at a constant rate $\gamma = A^{-1} dA/dt$.

Spreading rates are obtained by fitting observations of patch area to straight lines through each pair of points and for the sake of consistency using a linear regression (Fig. S3.1). The patch area

estimated from Fv/Fm is related to the initially fertilised area. Fv/Fm reacted to the addition of iron within hours and afterwards remained at approximately constant high values until the end of the experiment. From all variables measured in the field, Fv/Fm thus was the most direct and `conservative´ indicator of the iron supply.
The obtained dilution rates vary between 0.058 d^{-1} and 0.106 d^{-1} (Table S3.2). Because this range results from combining conservative and non-conservative properties, it likely overestimates the error of the dilution rate that can be determined from our assessment. Closest to each other are the dilution rates determined from the model (0.064 d^{-1}) and from combining the fertilised area and the Fv/Fm survey (0.068 d^{-1}). Using the horizontal diffusivity K_h = 56 $m^2 s^{-1}$ implied by the model (see caption Figure S5.1) to estimate the dilution rate as $\gamma = 2\ K_h / \sigma^2$, where σ^2 is the squared radial distance (12.4 km) yields 0.064 d^{-1}.

Table S3.2. Patch dilution rates (rates are in d^{-1})

Model	**Fv/Fm** Fertilization → Survey 2	**Chl** Survey 1 → Survey 2	***f*CO₂** Survey 1 → Survey 2
0.064	0.068	0.058	0.106

These patch dilution rates are a factor 6 – 12 higher than the dilution rates estimated for the core water mass of the eddy (Figs. S.3.2 and S3.3) due to mixing with water from the outside, either based on a horizontal diffusivity 87 $m^2 s^{-1}$ derived from the observed gradual warming of the eddy core[1] (0.008 d^{-1}, Fig. S3.3) or 0.009 d^{-1} determined by lateral stirring derived from altimetry-based eddy dynamics (Supplementary Information SI.2, Fig. S2.4). Note that while the horizontal diffusivities determined for the patch (56 $m^2 s^{-1}$) and for the eddy[2] (87 $m^2 s^{-1}$) differ by less then a factor of 2, the difference in dilution rates (about one order of magnitude) results from horizontal scales being roughly three times larger for the eddy compared to the fertilized patch.

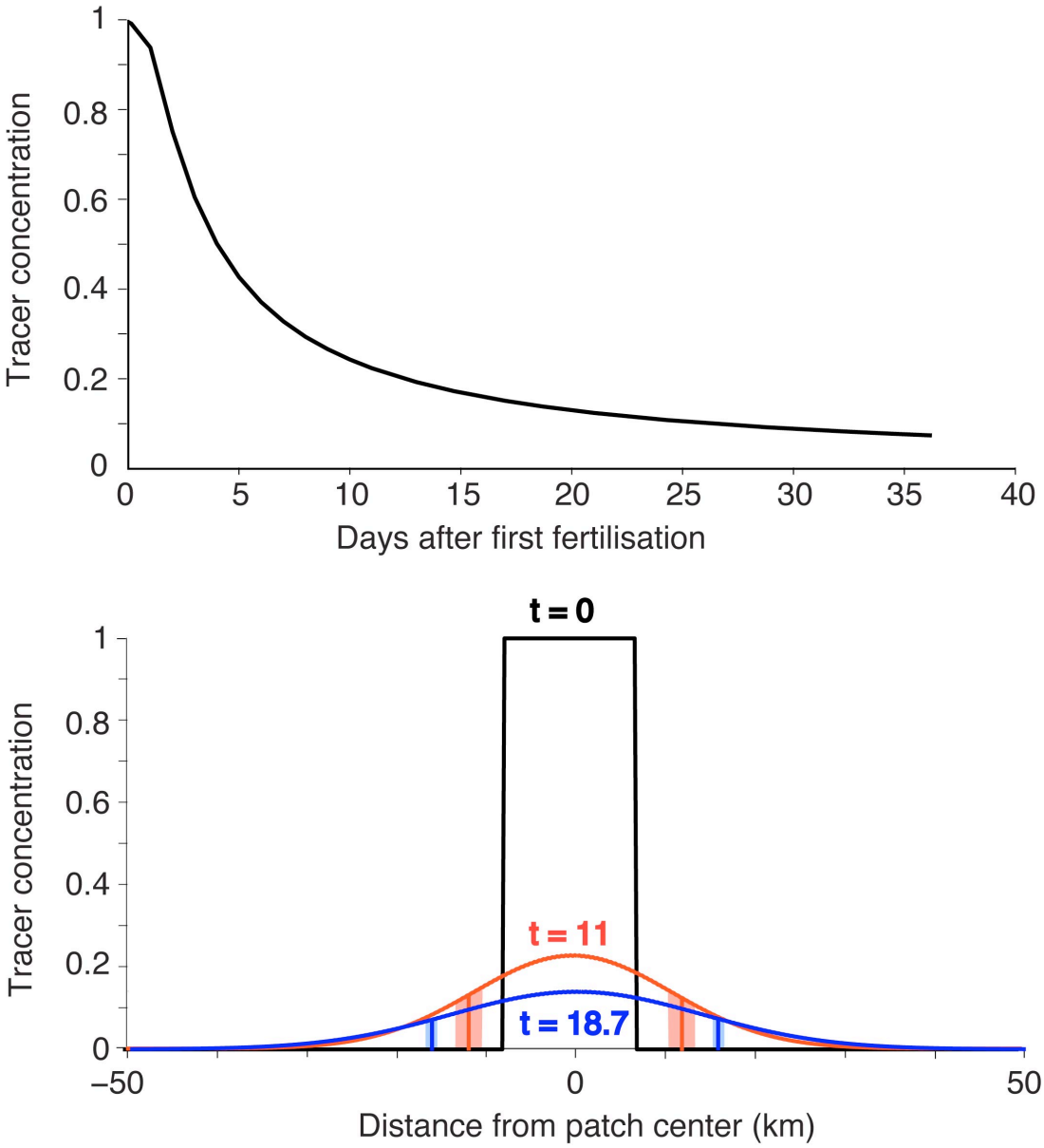

Figure S3.2. Patch dilution estimated based on a horizontal diffusivity of 56 m^2 s^{-1} assuming a uniform tracer concentration of 1 in the initially fertilized patch and zero concentration outside the fertilized patch. Upper panel: temporal decrease in tracer content in the centre of the patch (hotspot). Lower panel: radial tracer concentration initially (black line) during survey 1 (day 11, red line) and patch survey 2 (day 18.7, blue line). The average size and range of the patch determined from the distribution of Fv/Fm, Chl and fCO_2 (Table S3.1) are given by the horizontal lines and shaded areas for day 11 (red) and day 18.7 (blue).

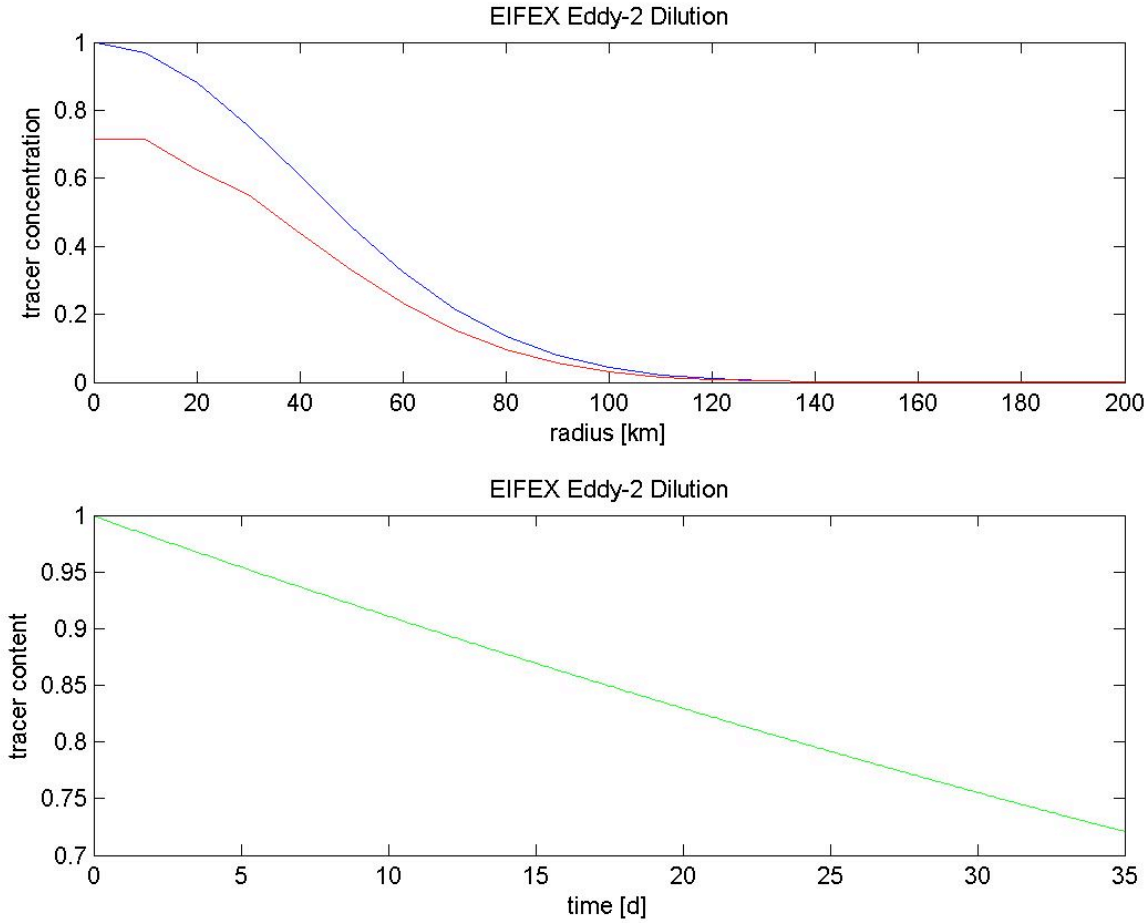

Figure S3.3. Eddy core dilution estimated based on the horizontal diffusivity obtained by Hibbert et al. (2009) assuming a passive tracer with Gaussian distribution centred at the eddy centre. Upper panel: radial tracer concentration initially (blue line) and after 35 days (red line). Lower panel: temporal decrease in tracer content of the eddy. According to these results, the tracer concentration in the eddy decreased by 28% during the 35 days. Assuming a linear decrease of tracer concentration, this can be translated into a dilution rate of 8 x 10^{-3} d^{-1}.

References for SI 3

1. Stanton, T. P., Law, C. S. & Watson, A. J. The physical evolution of the IronEx-I open ocean tracer patch, *Deep-Sea Res. II* **45**, 947-975 (1998).

2. Hibbert, A., Leach, H., Strass, V. & Cisewski, B. Mixing in cyclonic eddies in the Antarctic Circumpolar Current. *J. Mar. Res.* **67**, 1-23 (2009).

Supplementary Information SI 4
Patch dynamics and dilution

The same Lagrangian scheme employed in SI 2 is used to estimate the dilution of the fertilized patch under the effect of filamentation (due to lateral stirring) and diffusion (due to small-scale turbulence). In order to achieve this, we advect Lagrangian particles initially equally spaced at 0.001 deg. with the altimetry-derived velocity field plus a random noise with an intensity corresponding to a diffusivity of 56 m^2 s^{-1}. The advantage of this method is that no hypothesis is made on the shape that the patch maintains during its evolution. Some snapshots of the patch evolution, computed as the density of Lagrangian particles over a grid of 0.06 deg intervals are shown in Fig. S4.1. Particle number and grid size are chosen so that the particle density fluctuations over the grid due to the representation of diffusivity in terms of noise are negligible and so that patch filamentation can be fully resolved. The particle density is normalized so that a density of 1 corresponds to the undiluted fertilized patch. In agreement with the Lyapunov analysis of the eddy core evolution, stretching is very weak in the fertilized region and the patch maintains a regular and isotropic shape during its evolution. A weak stretching can be seen in Fig. S4.1 (lower right panel), when the patch starts to be skewed and the hotspot is a few km off from the eddy center. For each time of the simulation we measured the patch dispersion computing the standard deviation of particles composing the patch (white circles in Fig. S4.1). Figure S4.2 shows, in blue, the standard deviation of particle distribution, as a function of the days since fertilization. If only diffusion is active, the problem of a patch evolution in two dimensions has a well known analytical solution corresponding to:

$$C = C_0 \frac{\sigma(0)^2}{\sigma^2(0) + 2Dt} \exp\left[(x^2 + y^2)/(4Dt)\right].$$

Therefore, for this case the patch dispersion has a linear relation with the time:

$$\sigma^2(t) = \sigma^2(0) + 2Dt.$$

This Gaussian behaviour is shown by the red line in Fig. S4.2. The modelled patch deviates from the linear relation because of the presence of stirring, which stretches and skews the patch and amplifies the diffusivity due to small-scale turbulence. The dispersion is clearly super-diffusive after 35 days, when the patch develops some skewness and the Gaussian approximation for the standard deviation breaks down. The evolution of the hotspot (i.e., the maximal concentration of the patch) is indicated in Fig. S4.3. Again, the red line represents the dilution that is expected for a patch whose Gaussian evolution is determined by diffusion alone. In this case the maximum or hotspot concentration evolves as:

$$max\left[C\right] = C_0 \frac{\sigma(0)^2}{\sigma^2(0) + 2Dt} \sim \frac{1}{Dt}.$$

The hotspot (blue line in Fig. S4.3) closely follows a Gaussian behaviour and is less affected by stirring than the standard deviation. The model estimates the hotspot dilution is 26%, 13%, 9.5% and 0.075% after respectively 10, 20, 30, and 40 days. Also note that if the patch had been released in a region of more intense stirring, such as at the eddy periphery, the filamentation process would have started to dominate over the Gaussian behaviour from the beginning of the experiment, and the patch would have been dispersed after a few days.

In conclusion, the altimetry-based Lagrangian analysis of the patch filamentation indicates that:

- The patch was in a region of very weak filamentation for the entire duration of the experiment.
- The fertilized patch maintained a Gaussian shape until day 35.
- Lateral stirring skewed the patch but had a negligible effect on the hotspot dilution rates, which was almost completely controlled by small-scale diffusion.

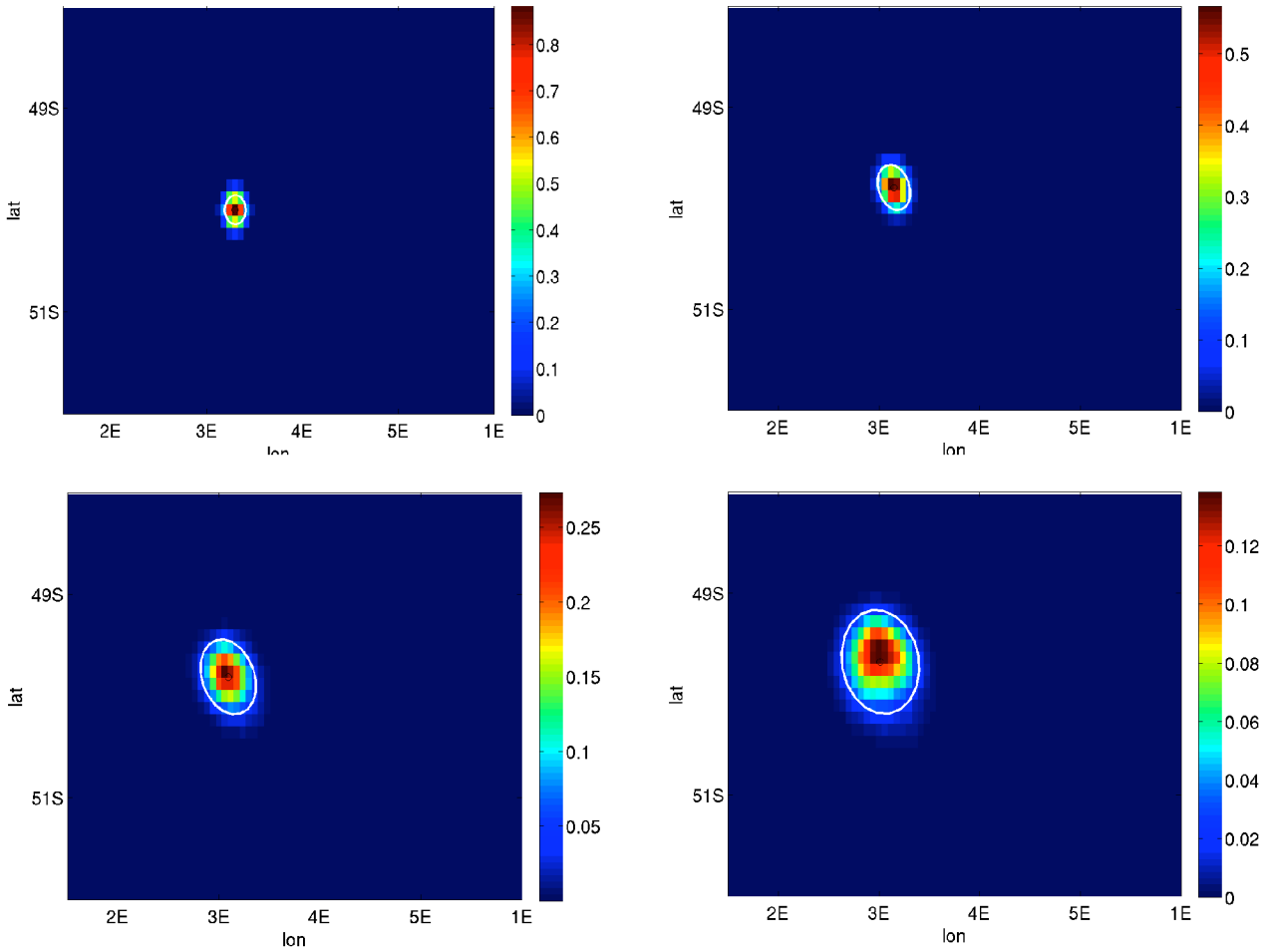

Figure S4.1. Evolution of the fertilized patch modeled using Lagrangian particles, altimetry-derived velocity and random noise corresponding to a diffusivity D = 56 m^2 s^{-1}. Distribution of particle density is given after 1 (upper left panel), 2 (upper right panel), 8 (lower left panel), and 16 days (lower right panel) after fertilization.

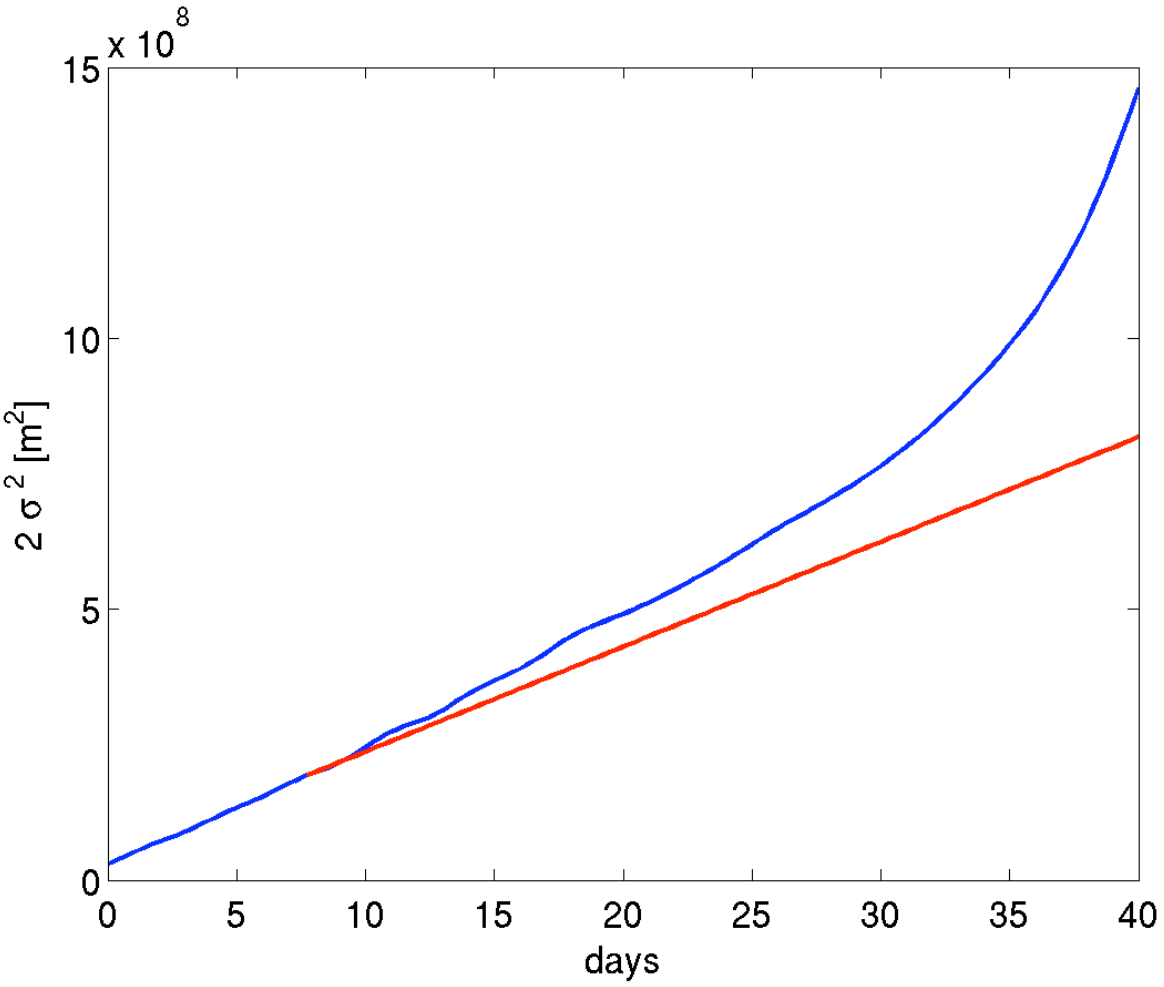

Figure S4.2. Fertilized patch dispersion as a function of time. The red line shows the evolution of the standard deviation of a Gaussian patch under the effect of a diffusion D = 56 m^2 s^{-1} and without advection. The blue line shows the standard deviation observed in the model, in which both diffusion and advection are considered.

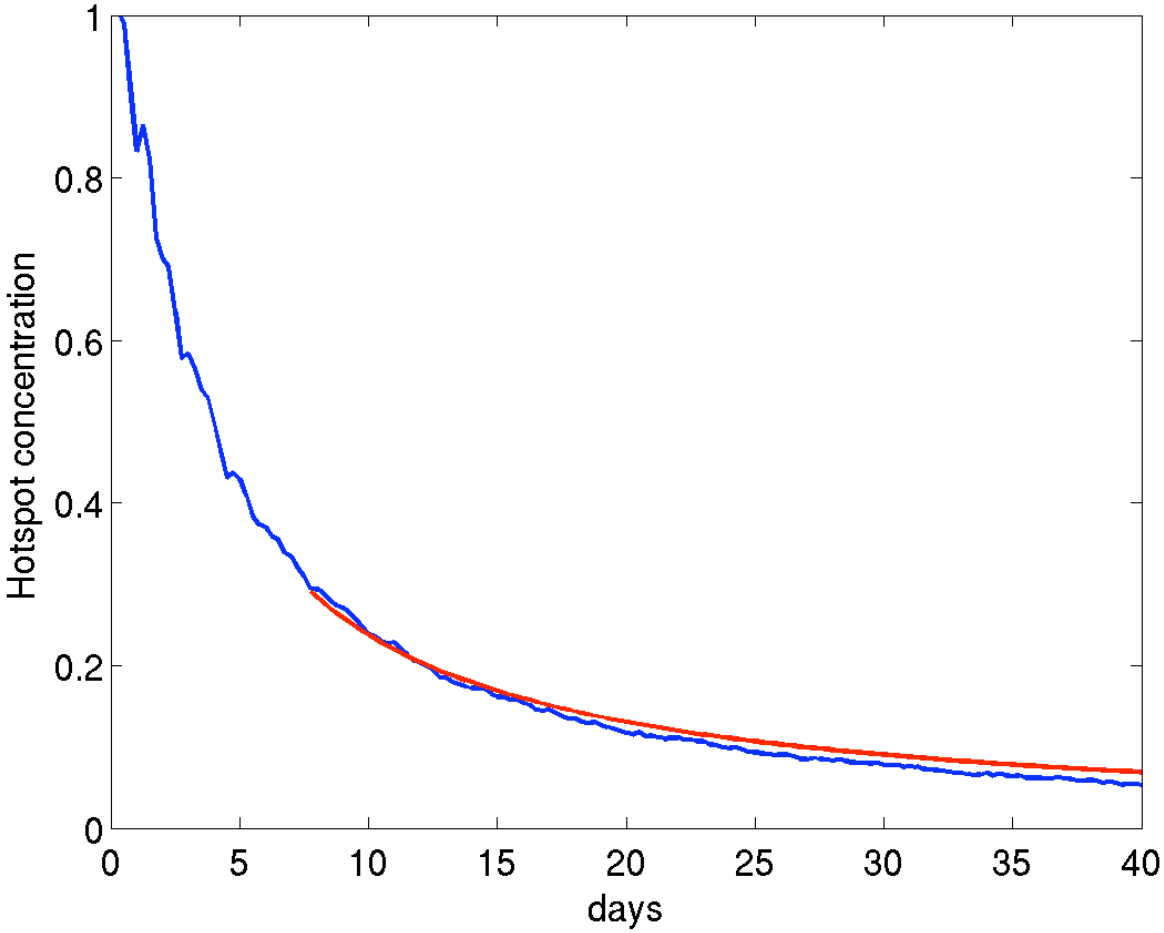

Figure S4.3. Evolution of the hotspot particle concentration as a function of time. The red line shows the evolution of the maximum concentration of a Gaussian patch under the effect of a diffusivity D = 56 m^2 s^{-1} alone. The blue line shows the maximum (hotspot) concentration observed in the model, in which both diffusion and advection are considered.

Supplementary Information SI 5
Iron-induced and background export

Export from natural vs. artificial blooms

The Antarctic Zone is the least productive belt of the ACC with Chl concentrations typically <0.2 mg Chl m^{-3}. Hence, the concentrations prevailing in the eddy core in the region of the patch prior to fertilization (~0.7 mg Chl m^{-3}) are elevated and the patches in the core with twofold higher concentrations can be accorded the status of minor blooms. The Antarctic Polar Front on the other hand is the most productive zone of the ACC presumably due to dust deposition caused by higher rainfall levels along this weather front. Ship-borne observations indicate that precipitation events tend to be local and short which would explain the patchiness within the eddy core. Further to the West, dust input from iceberg melting can be a significant source of iron but icebergs were absent in the EIFEX eddy.

Our observations indicate that export from the 3 biomass levels encountered during EIFEX: the 0.7 Chl mg m^{-3} pre-fertilization situation, the >1.0 mg minor, natural blooms in the eddy core and the 2.8 mg Chl m^{-3} reached at the peak of the EIFEX bloom varied with regard to the rate of sinking and the depths reached by the sinking particles prior to remineralisation. The common feature is that the carbon missing from the surface layer was not respired within it but exported to successively deeper layers depending on the biomass levels of the diatom stocks. Apparently the surface regenerating community has an upper threshold of retention beyond which "excess" POC, contributed by diatoms in the presence of silicate, eventually settles out together with the iron on which the production was based. This is consistent with the short life-time of iron introduced from dust or from shelf sediments to the surface layer[1,2] and implies that, at least in the case of diatoms, the iron is lost together with organic matter at high C:Fe ratios[3].

Similarly, there will also be an upper threshold on the ability of the subsurface heterotrophic community to respond to an increase in the food supply dictated by their respective intrinsic growth rates. Thus, export from lower biomass levels was respired in the upper few 100 m within days as the accumulation rate was <10 % of export. In contrast, sinking POC from the intermediate biomass level (natural blooms) had a much longer life-time (weeks) in the water column. Vertical flux from these minor blooms was slower than from the EIFEX bloom, presumably because the lower concentrations of the former resulted in smaller aggregates. Nevertheless, the bulk of biomass from these natural diatom blooms apparently also sank deep. Export from the EIFEX bloom lost an even smaller percentage of POC to respiration underway. Similarly, the extensive bloom present in the APF meander prior to our arrival had not only disappeared from the surface, but from the entire water column some 2 weeks later when the grid was conducted (Fig. S1.2). It is likely that the entire 1.8 mol C m-2 which accumulated in the water column during EIFEX sank out of it within weeks of our departure. In conclusion, subsurface respiration of sinking particles increases with the magnitude of flux up to a threshold beyond which the bulk of the flux settles out of the water column. Testing this hypothesis and estimating the response rates of the subsurface heterotrophic community to increasing flux could be one of the foci of future experiments.

Our observations are consistent with the conclusions drawn from excess barium profiles taken during EIFEX[4] which is a proxy for carbon remineralisation rates. The authors estimated rates ranging between 14 and 96 mg C m^{-2} d^{-1} (1.2 – 8 mmol) for the 150 – 1000 m water column inside and outside the patch whereby the highest values were recorded on days 28 in-patch (at the start of the iron induced flux) and on day 34 out-patch (in the site of the natural bloom). Interestingly, rates

at the pre-fertilization station were also high (6.5 mmol C m^{-2} d^{-1}). Nevertheless, they are rather low to account for the average uncorrected, background exports estimated from nutrient budgets of 12 and 21 mmol C m^{-2} d^{-1} inside and outside the patch respectively; comparison with values corrected for diapycnic mixing (26 and 36 mmol C m^{-2} d^{-1} respectively) exacerbates the problem, indicating that corrected values are overestimates of background flux. This does not apply to iron-induced exports of 79 and 98 mmol C m^{-2} d^{-1} (uncorrected and corrected respectively) which are 90 % higher than maximum respiration rates and consistent with POC accumulation in the deep water column. However, it should be pointed out that the interpretation by Jacquet et al.[3] of the high out-patch value on day 34 as stemming from the iron-induced bloom was based on a preliminary assessment of the circulation regime within the eddy core. The analyses now presented here all indicate vertically coherent circulation and identify pre-fertilization natural blooms (also reported by Jacquet et al.) as the origin of the high out-patch POC stocks at depth.

Thorium

The flux event from the fertilized patch also appeared as a strong signal in disequilibrium of naturally occurring, radioactive, particle-active ^{234}Thorium relative to the parent, particle-neutral ^{238}Uranium. Before the flux event, thorium loss rates converted to carbon from the patch were fairly constant (28.3 ± 1.4 mmol C m^{-2} d^{-1}) and similar to outside water and about half the estimate from the corrected carbon budget. During the flux event, rates increased fivefold to a maximum of 141 ± 51 mmol C m^{-2} d^{-1} (1.7 g C m^{-2} d^{-1}), the highest carbon export flux recorded to date from the Southern Ocean by this method, but declined on the last day although all other measurements indicate ongoing vertical flux. According to the thorium data a total of 0.65 ± 0.18 mol C m^{-2} is estimated to have sunk out of the upper 100 m layer from day 24 to day 36 inside the patch. In view of the twofold lower C/Si ratio due to higher contribution of empty diatom frustules to total flux[16] of out-patch and in-patch background fluxes (based on elemental budget calculations) as compared to iron-induced fluxes, the assumption of constant POC:^{234}Th of sinking particles might not be valid. Hence, carbon flux outside the patch and between day 0 to 24 in patch might have been overestimated relative to iron-induced fluxes.

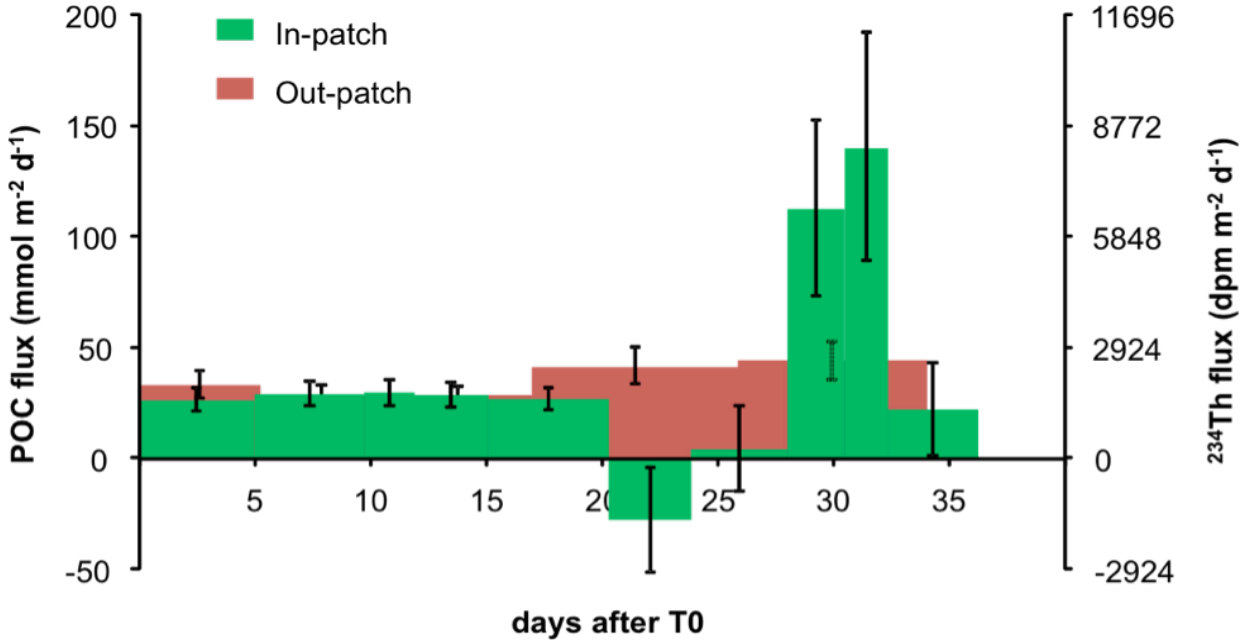

Figure S5.1. Fluxes of ^{234}Thorium and ^{234}Th-derived POC fluxes as function of time (days after first fertilization). In-patch (hot-spot) values are given by the green bars and out-patch values by the red bars. Error bars (in black) represent 1 standard deviation.

C/Fe ratios of the EIFEX bloom

The C/Fe ratio of 13,000 ± 1000 presented in the main text is an underestimate for the following reasons: a) Fv/Fm values did not change until the end of the experiment implying that hotspot phytoplankton had not yet reached iron limitation; b) the iron added during the second fertilization remained in the water column as dissolved iron for several weeks (Fig. S5.2) and the increase in dissolved iron concentrations below 100 m depth (Fig. S5.2) indicates that much of the iron from the second fertilization was lost through physical processes; c) enhanced primary production and carbon uptake and fluxes continued after we left the eddy.

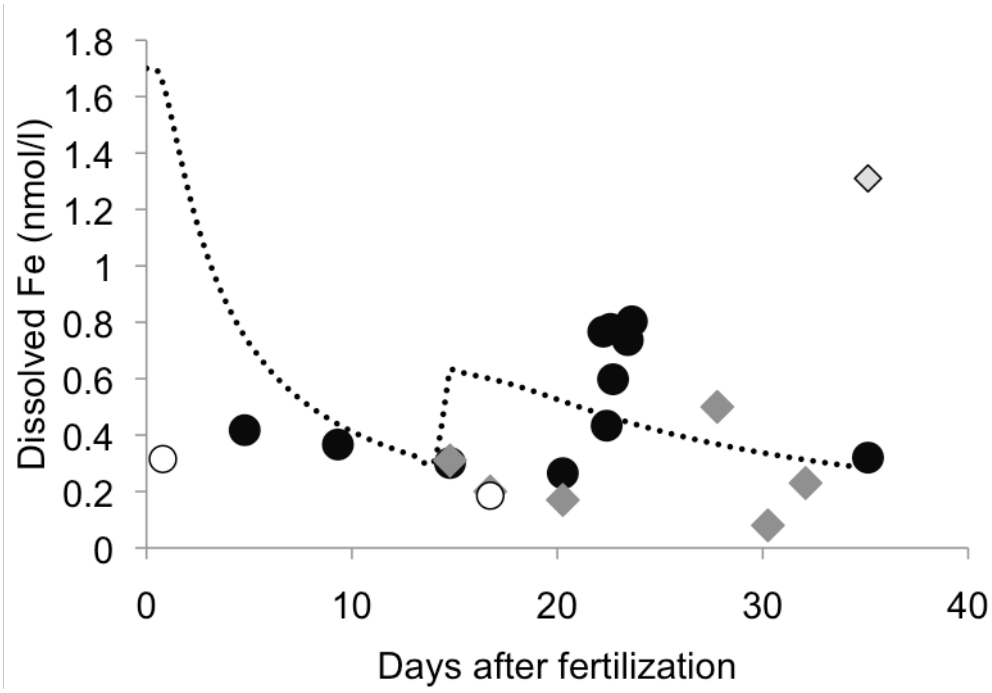

Figure S5.2. Dissolved iron concentrations as function of time (days after first fertilization). Average surface layer (0-100 m) in-patch values are given by the filled circles and out-patch values by the open circles. Mean concentrations in deeper layers (120-150 m) are shown by grey diamonds. Theoretical dissolved iron curve (dotted line) shows the dissolved iron evolution in the hot-spot assuming no uptake and a horizontal diffusivity of 56 m^2s^{-1}. The high value at 150 m on day 35 is probably an outlier.

We employed an alternative approach to estimating the C/Fe ratio of biomass built up by fertilization: We estimated the total amount of chlorophyll in the 100 m surface layer of the patch after it had spread to 798 km^2 during the second mapping on days 17 – 20 using 1.0 mg Chl m^{-3} as the outer boundary of the patch. If, in a thought experiment, this amount is compressed into the 167 km^2 area initially fertilized, we obtain a standing stock of 900 mg Chl m^{-2} which is three times the stock measured in the hotspot a day later. POC in the hotspot water column integrated to 3,000 m depth continued increasing at the same rate until the end of the experiment, implying that the rate of biomass accumulation did not change. We extrapolate the increase from day 0 – 20 to day 36 and obtain a hypothetical standing stock in the initial patch of 1600 mg Chl m^{-2}. Converted into POC using the C/Chl (mg/mg) ratio of 32 we obtain 50 g C m^{-2} or 4.2 mol C m^{-2} which yields a C/Fe

ratio of 23,000. This ratio is still an underestimate because the 1 mg Chl m^{-3} cut-off is well above Chl concentrations prevalent in outside water at the time (0.6 mg Chl m^{-3}). Based on these considerations we estimate that C/Fe ratios in all probability were closer to 30,000 than the 13,000 estimate presented in the main text.

References for SI 5

1. Blain, S., et al. Effect of natural iron fertilization on carbon sequestration in the Southern Ocean. Nature 446, 1070-1075 (2007).

2. Pollard, R., et al. Southern Ocean deep-water carbon export enhanced by natural iron fertilization. Nature 457, 577-580 (2009).

3. Sarmiento, J. L., Slater, R. D., Dunne, J. P. & Hiscock, M. R. Efficiency of small scale carbon mitigation by patch iron fertilization. *Biogeosciences*, **7**, 3593-3624 (2010).

4. Jacquet, S. H. M., Savoye, N., Dehairs, F., Strass, V. H. & D. Cardinal, D. Mesopelagic carbon remineralization during the European Iron Fertilization Experiment. *Glob. Biogeochem. Cycles.* **22**, GB1023, doi:10.1029/2006GB002902 (2008).